EVALUATION OF THE OSTEOIMMUNOMODULATORY PROPERTIES OF SURFACE BIOFUNCTIONALIZED 3D PRINTED TITANIUM BONE IMPLANTS

AMAIA GARMENDIA URDALLETA

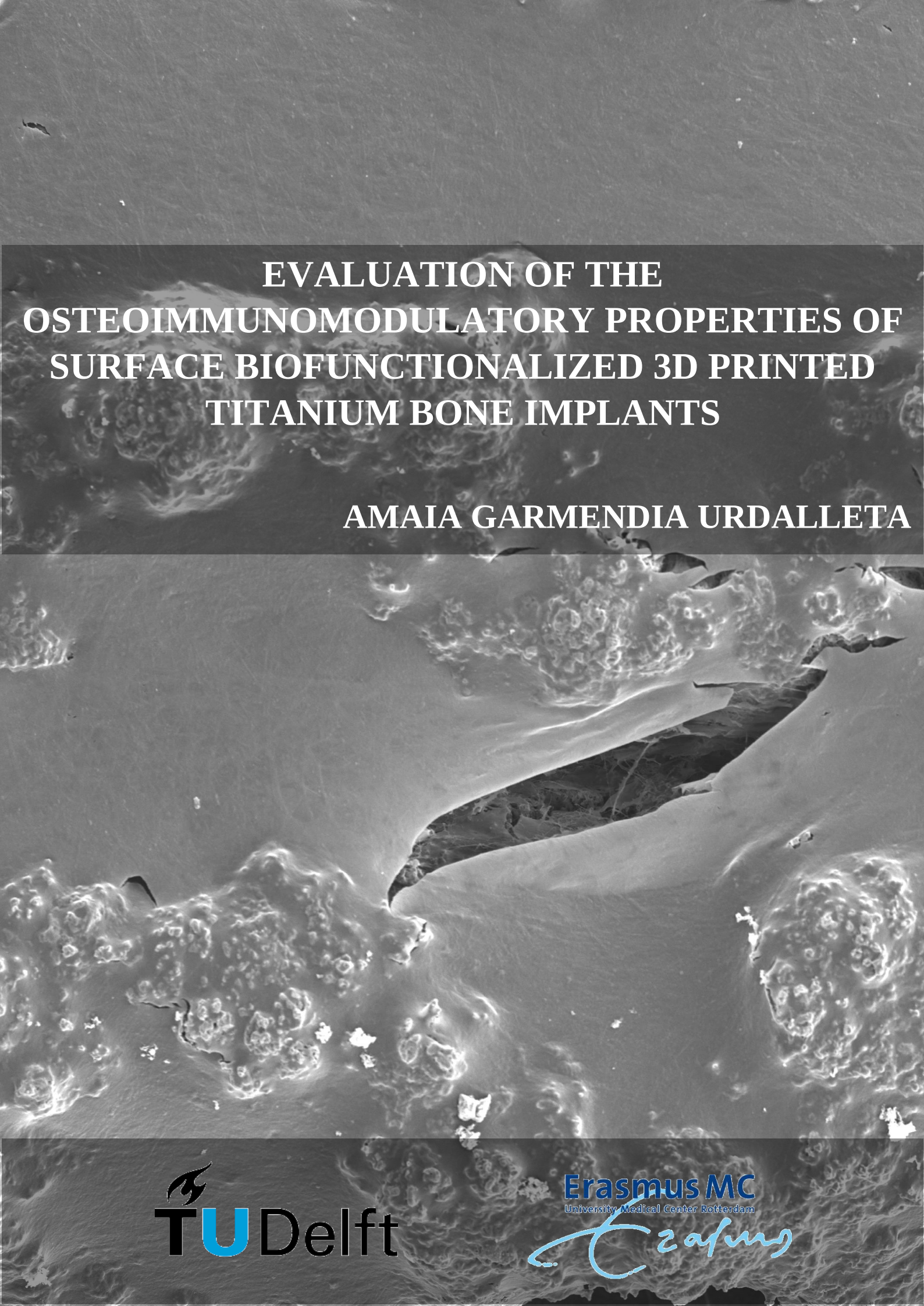

TU Delft

Erasmus MC
University Medical Center Rotterdam

EVALUATION OF THE OSTEOIMMUNOMODULATORY PROPERTIES OF SURFACE BIOFUNCTIONALIZED 3D PRINTED TITANIUM BONE IMPLANTS

By

Amaia Garmendia Urdalleta

5126703

In partial fulfilment of the requirements for the degree of

Master of Science

In Biomedical Engineering

At the Delft University of Technology,

To be defended publicly on Tuesday September 28, 2021 at 11:00 AM

Supervisors:

Dr. ir. E.L. Fratila-Apachitei (TU Delft)

Dr. E. Farrell (Erasmus MC)

Prof. Dr. Ir. A.A. Zadpoor (TU Delft)

Biomaterials and Tissue Biomechanics Section

Biomechanical Engineering Department

Faculty of Mechanical, Maritime and Materials Engineering

Delft University of Technology

ABSTRACT

Background. Despite the considerable development of the field of orthopedic implants in the past century, complications including poor bone ingrowth and implant associated infection (IAI) persist to this day, causing a huge burden to millions of patients and the healthcare systems worldwide. Additive manufacturing (AM) and the subsequent surface biofunctionalization and antibacterial element incorporation are promising techniques to achieve dual antibacterial and osteogenic functionalities within a bone implant. In addition, macrophages are an immune cell type that are known to be essential for the implant success in the body, by having an intimate crosstalk with mesenchymal stem cells (MSCs) in the process of new bone formation. However, the behaviour of these immune cells is affected by environmental cues, including the implant surface properties. Therefore, this work investigated for the first time the effects of AM titanium implants biofunctionalized via plasma electrolytic oxidation (PEO) and incorporated with silver nanoparticles (AgNPs) on the human mesenchymal stem cells (hMSCs) co-cultured *in vitro* with human macrophages. Specifically, the paracrine effects of immune cells on the hMSCs osteogenic differentiation were studied by the development of an indirect co-culture model.

Materials and methods. AM Ti-6Al-4V implants were biofunctionalized via PEO and AgNPs incorporation and the surface characterization was performed by a scanning electron microscope (SEM) and ion release analysis. The effects of such implants on the hMSCs osteogenic differentiation *in vitro* were subsequently evaluated by measuring the mineralization and osteogenic gene expression. In addition, a macrophage-hMSCs indirect co-culture system was developed in order to study the effects of the macrophage polarization induced by the implants on the hMSCs osteogenic differentiation by means of a paracrine communication. The macrophage polarization was characterized by measuring the cytokine secretion pattern with an ELISA assay and gene expression.

Results. PEO modification of AM implants created TiO_2 surfaces with interconnected micro and nanoporosities and the incorporation of AgNPs. The single-culture of hMSCs on PEO and PEO + Ag implants revealed their ability to promote the osteogenic differentiation and no detrimental effects were observed in this process by the presence of AgNPs. The immunological evaluation of the co-culture system revealed similar polarization patterns when macrophages were cultured on PEO and PEO + Ag surfaces. In addition, factors secreted by polarized macrophages did not elicit a paracrine effect on the co-cultured hMSCs, neither enhancing nor inhibiting their osteogenic differentiation.

***Discussion and conclusions*.** Based on the findings gathered in this study, the incorporation of AgNPs in the PEO layers, under the conditions used in this work, did not compromise the osteogenic differentiation and mineralization of the hMSCs. In addition, PEO + Ag surfaces did also not cause any detrimental effects on the paracrine communication of human macrophages on hMSCs. Therefore, further investigations regarding the osteoimmunomodulatory potential of these biofunctionalized AM implants are worth performing, in an attempt to achieve an important additional biofunctionality next to their proven osteogenic and antibacterial activity. These future researches should include further optimization of the PEO surface morphology and chemistry as well as the co-culture model used in this study.

ACKNOWLEDGEMENTS

First of all, I want to thank Dr. ir. Lidy Fratila-Apachitei for giving me the opportunity to work in such a multidisciplinary, challenging and very interesting project. Her constant critical and enthusiastic feedback as well as her motivating and encouraging words were always infinitely helpful for pushing me to give my best in every step of this research study, even when the light at the end of the tunnel seemed to be kilometres away from me.

A big big thank you to Dr. Eric Farrell for being so patient with my frustrations and tons of questions every day. His critical and very useful feedback has made me learn to think out of the box and his very wise guidance this past year has immensely contributed to my growth both in a professional and personal level.

Thanks a lot to all the members of the labs in both Erasmus MC and in the Biomechanical Engineering Department in TU Delft for welcoming me so warmly to the team and being so helpful, supportive and encouraging in this journey. I would like to especially thank Janneke for all help in the lab, the many many teaching sessions and constantly answering to my daily doubts. Special thanks also to Niamh who guided and supported me for a big part of this project with great enthusiasm. Finally, thanks to Monika for her infinite help, encouraging words and very useful feedback.

I am deeply grateful to my parents for their continuous support, patience and encouragements as well as to my sister, aunt and cousins for all the love they send me. I would not be here without them. A big thank you to my 'girls' back home and to Paula, who despite the distance is always happy to hear my news and sends me tons of doses of positivity.

Finally, thanks to my beloved 'Simons' housemates. I never thought that choosing this house was going to give me two of the most amazing years of my life, with so many incredible moments and friendships for life. Thanks also to my master friends for making my 'Delft experience' unforgettable.

Content

1. INTRODUCTION

The development of orthopedic implants in the mid-20th century presented an important breakthrough in the medical field because it suddenly returned the mobility to thousands of people [1]. Titanium was and is still the material par excellence for oral and orthopedic implants due to the interesting properties it possesses, including chemical biocompatibility, mechanical properties and resistance to corrosion [2, 3]. However, those primitive structures were far from perfect, having many issues and a limited lifespan. Despite the major advances and efforts in the field, some of those complications including poor bone ingrowth and IAI [4] still persist to this day causing a huge burden to millions of patients and the healthcare system [5]. In addition, the use of orthopedic implants in the medical field is steadily increasing every year. For example, the number of total hip replacements (THR) in the Netherlands has increased by 30% since 2010 [4].This trend is expected to continue in the next decades due to population aging and improvements in medical care [2]. As such, the development of biomaterials that can support the integration of the implants in the host body without creating adverse effects is an important current research domain [6]. New implant surface design methods are being actively developed and pursued to improve the clinical outcomes of implants.

Among these novel methods, AM has shown promising results. This technique now enables the fabrication of metallic implants with easily tunable designs and microarchitecture. In particular, an increase in surface roughness and area can be achieved as a result of the increased macroporosity of 3D printed structures [7]. Studies have demonstrated that a bigger surface area enhances bone forming cell adhesion and differentiation, eventually stimulating the osteogenic differentiation of MSCs [8–10]. These multipotent cells are able to differentiate into several types of cells, including bone [11]. In addition, biofunctionalization techniques also enhance surface bioactivity and roughness, and are often required to achieve a complete osseointegration, which is not possible with AM alone [12]. However, the increase of the surface area means that the probability of bacterial invasion during surgery is higher, which can subsequently lead to complications and implant failure [13]. Therefore, the further biofunctionalization of implants by the incorporation of antibacterial elements is a vital step forward for the creation of suitable metallic bone substitutes. Extensive research has been performed in order to combine dual antibacterial and osteogenic functionalities within an implant [14–17]. Nevertheless, neglecting the vital role that immune cells have within the bone healing process after implantation and following the traditional strategy of fabricating inert biomaterials that minimize immune reactions has proven to be insufficient [18–20] with many implant candidates failing to reach clinical use.

In recent years, researchers have started acknowledging the key role of the immune system in bone homeostasis (Figure 1). Biomaterial implantation in the body is followed by an initial plasma protein adsorption and coagulatory cascade. Next, an acute inflammatory response is initiated via the release of cytokines and chemokines from damaged cells [21, 22]. Neutrophils are first recruited followed within 24-48 hours by monocytes. When reaching the implant site monocytes differentiate into macrophages and become activated. The macrophage polarization pattern is a continuum spectrum but two fundamental states exist [23]: Classically activated/M1, which secrete pro-inflammatory cytokines and play a key role in the early stage of inflammation by eliminating external pathogens, or alternatively activated/M2, characterized by the secretion of anti-inflammatory cytokines while enhancing tissue repair (Figure 2). Both polarization states are necessary but it is only when a fine balance is maintained that macrophages can release osteogenesis-enhancing factors,

angiogenic factors and recruit MSCs, leading to a successful new bone formation [24–26] In addition, the evidence of macrophages' sensitivity to environmental cues [27], demands an adequate adjustment of the osteoimmunomodulatory surface properties of biomaterials including chemical composition, wettability or topography which can result in a desired macrophage polarization pattern and subsequent osteogenesis [28, 29].

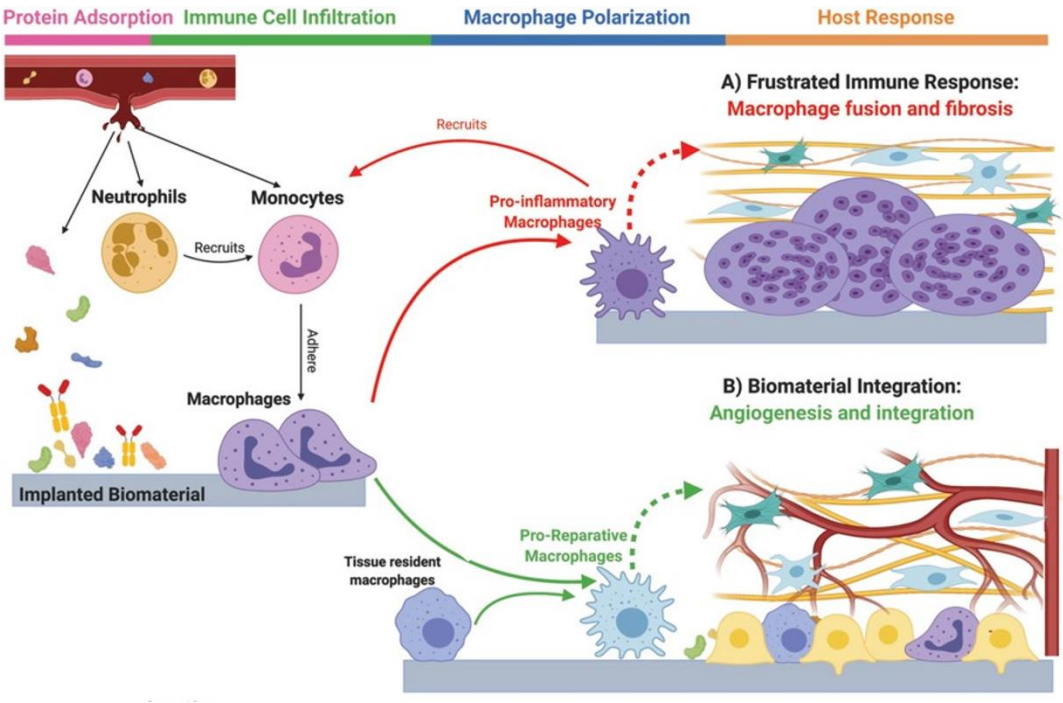

Figure 1. Schematic illustration of the role of immune cells in the biomaterial implantation in the body and new bone formation. First, plasma proteins adhere to the biomaterial and neutrophils infiltrate into the wound, followed by monocytes. After an initial inflammatory stage, if macrophages persist with their pro-inflammatory cytokine release, eventually fibrous encapsulation will happen. However, if they switch towards a pro-regenerative phenotype, new bone will be formed, and the biomaterial will be successfully implanted into the body. Figure adapted form [23].

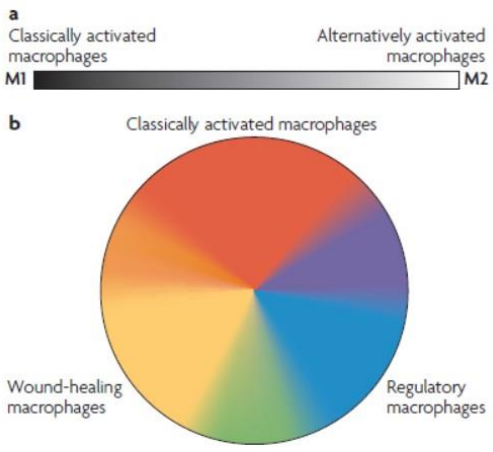

Figure 2. Macrophage polarization spectrum. A) Monochromatic depiction of the two fundamental macrophage states, M1 and M2. B) Color wheel of the macrophage activation pattern showing the continuum spectrum of the macrophage populations that exist [25].

The majority of the *in vitro* models developed for the study of the effect of modified titanium surfaces on monocytes/macrophages [30, 31] or stem cells [32–34] are based on single-cell type models. However, the studies investigating titanium modifications on 'multi-cell type' interactions between stem cells and immune cells are very scarce [35, 36] and practically non-existent for modified AM porous titanium implants. Therefore, further investigation in this area is needed.

In this work the effect of biofunctionalized AM porous titanium implants on the hMSCs co-cultured *in vitro* with human macrophages was studied for the first time. Specifically, the focus was given to studying the paracrine effects of immune cells on the hMSCs osteogenic differentiation by developing an indirect co-culture model (Figure 3). AM implants were modified by PEO, incorporating also AgNPs. The resulting highly porous surfaces contained calcium phosphates and AgNPs, making the implant more osteogenic as well as minimizing the risk of IAIs and having potential immunomodulatory effects as shown in previous studies using monocultures [20, 34, 37].

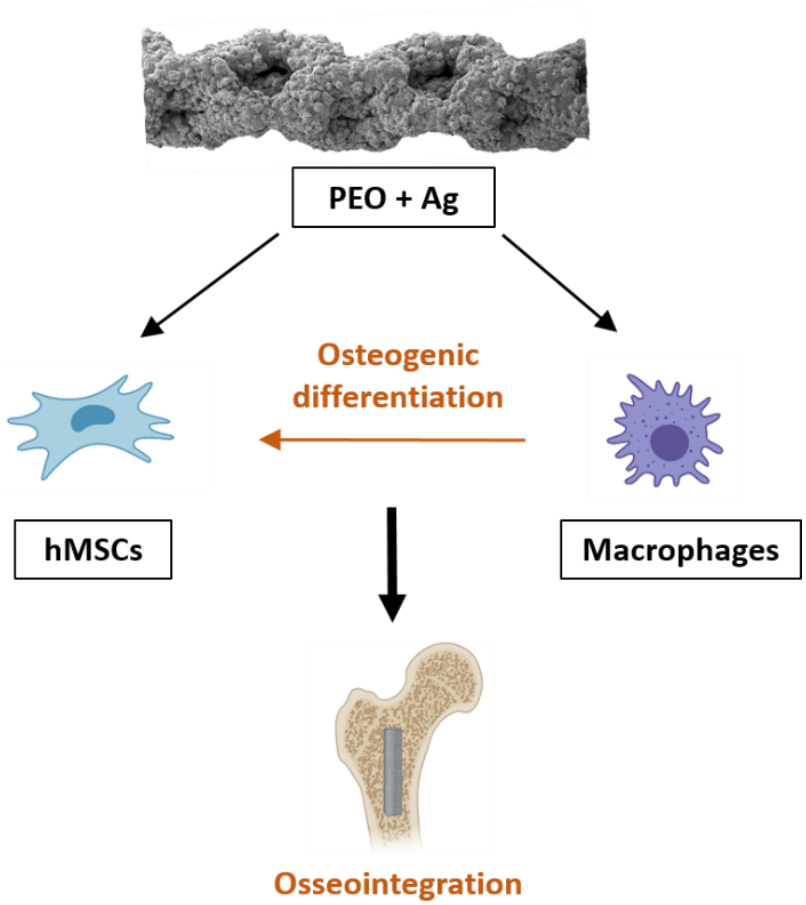

Figure 3. Osteoimmunomodulation paradigm. In this study, the effects of implants treated with PEO and incorporated with AgNPs on the hMSCs co-cultured *in vitro* with human macrophages were evaluated.

Following the AgNPs-incorporated PEO implant fabrication, biofunctionalization and characterization by SEM and ion release analysis, the effects of such surfaces on the hMSCs osteogenic differentiation and matrix mineralization were evaluated by means of various assays including measuring the calcium concentration in the medium, xylenol orange labelling or osteogenic gene expression analysis (Figure 4). After that, the same osteogenic evaluation of hMSCs was performed but when co-cultured with macrophages. The macrophage polarization pattern was measured by performing a quantification of the cytokine secretion and the measurement of the expression of certain immunological genes.

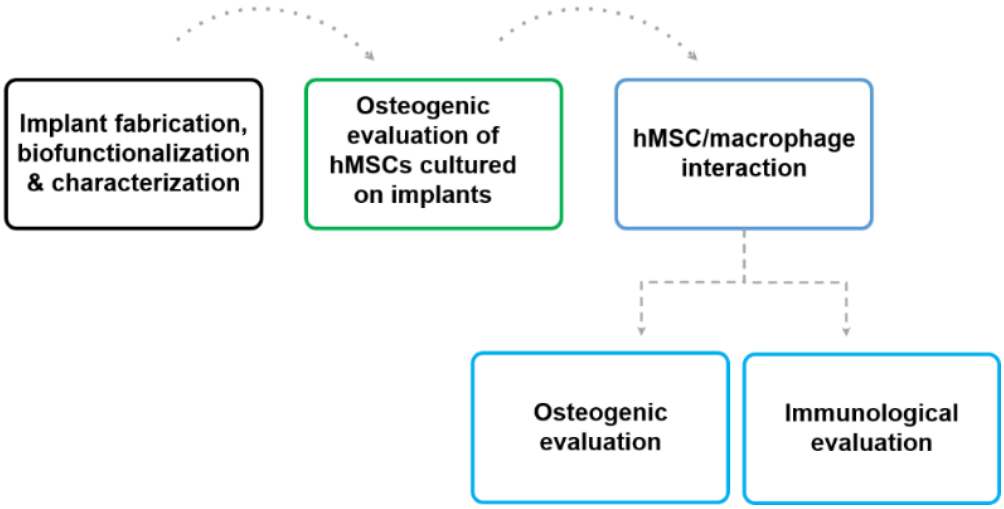

Figure 4. Schematic diagram of the research outline.

2. MATERIALS AND METHODS

2.1 Ti-6Al-4V implant design and fabrication

Ti-6Al-4V implants were previously fabricated following a pre-established design rationale and protocol [34] with the aim of promoting bone ingrowth by increasing the surface area, roughness and porosity. Fabrication took place in the Additive Manufacturing Laboratory (TU Delft, Delft, The Netherlands) by means of a SLM printer (SLM-125, Realizer, Borchem, Germany) that operated with a YLM-400-AC Ytterbium fiber laser (IPG Photonics Corporation, Oxford, United States) under an atmosphere containing argon and an oxygen content of less than 0.2%. Medical grade (grade 23, ELI) Ti-6Al-4V powder particles (APC, Boisbriand, Quebec, Canada), which were spherical and with particle sizes of 10-45 μm were used. Following fabrication, vacuum cleaning and ultra-sonication in acetone, 96% ethanol, and demineralized water was performed in order to remove any possible loose particles that were created during the 3D printing process. The resulting structures were 40 mm long and 0.5 mm wide, with a pore length of 360 μm and pore width of 230 μm (Figure 5).

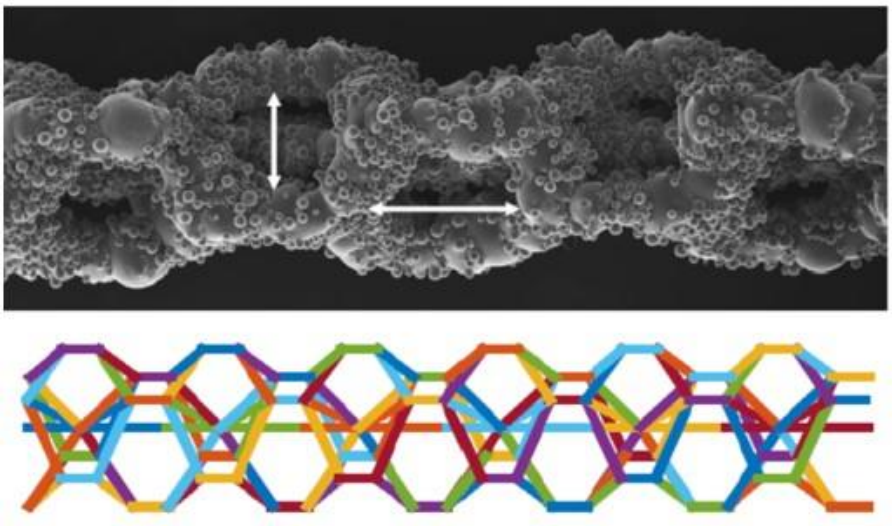

Figure 5. SLM Ti-6Al-4V porous implants after fabrication, with their characteristic design and morphology and pore length and width shown in white arrows. Figure adapted from [34].

2.2 Surface biofunctionalization via PEO

2.2.1 Fundamentals of the PEO process

AM implants were biofunctionalized by PEO. This technique, also called micro-arc oxidation (MAO), is an electrochemical surface treatment that generates porous oxide layers on the surface of certain metals [38]. The applied surface modification can be modulated by changing the process parameters such as the applied current, time and electrolyte composition having an influence on the final achieved surface properties. In the case of titanium-based materials such as Ti-6Al-4V, the applied high constant current causes the native titanium oxide (TiO_2) layer to vastly expand in the first few seconds of the process, causing the voltage to increase linearly (Figure 6). The potential difference between both sides of the oxide layer keeps increasing until the breakdown potential is reached. At this point the weakest points in the structure, which have the lowest resistance, suffer a dielectric breakdown and discharges occur, resulting in localized plasma formation, sparks and high local temperatures [12].These phenomena lead to the formation of pores in the newly formed titanium oxide layer [39].

In addition to creating a highly porous layer, different elements added in the electrolyte such as calcium (Ca) or phosphorus (P) can be incorporated into the oxide layer, further enhancing the biocompatibility of implants. Moreover, antimicrobial elements can also be added to the electrolyte, such as AgNPs that become entrapped on the porous layer and prevent biofilm formation by the local release of Ag+ ions which is sustained in time [40].

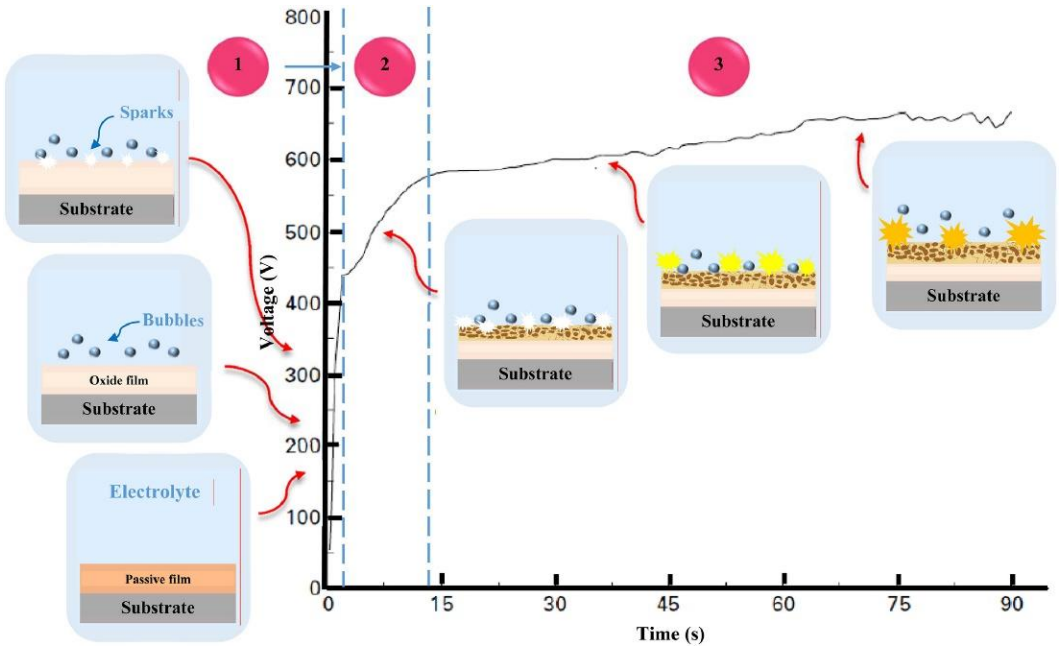

Figure 6. Voltage-time graph showing the different steps involved in the creation of a porous oxide layer by PEO. Step 1 shows the growth of the dense oxide oxide layer creation phase, while in step 2 and 3 the dielectric breakdown results in local plasma and sparks formation as well as the creation of pores by the release of oxygen [41].

2.2.2 PEO-modification of Ti-6Al-4V implants

Ti-6Al-4V implants were treated in two different ways, resulting in two experimental conditions: 1) PEO-modified implants (i.e. PEO group) and 2) PEO-modified implants with the incorporation of AgNPs (i.e. PEO + Ag group).

Biofunctionalization took place in the Surface Biofunctionalization Lab (TU Delft, The Netherlands) by means of a PEO research unit which included an AC power supply (50 Hz, type ACS 1500, ET Power Systems Ltd, Eyam, United Kingdom), a data acquisition board (SCXI, National Instruments, Austin, Texas, United States), a computer interface, a thermostatic bath (Thermo Haake V15, Karlsrhue, Germany) and an electrolytic cell made of double-walled glass, which contained 800 ml electrolyte (Figure 7). The AM titanium implants represented the anode and a stainless steel cylinder was used as the cathode.

The PEO electrolyte contained 24 g/L calcium acetate (CaA), 4.2 g/L calcium glycerophosphate (CaGly) and for the PEO + Ag implants, spherical AgNPs in a concentration of 0.3 g/L (Sigma-Aldrich, St. Louis, Missouri, United States) and with sizes varying between 7 and 25 nm were added to the electrolyte. When AgNPs were to be incorporated into the implants, they were added to the electrolyte and the solution was

sonicated 2 times for 5 minutes and stirred inbetween for 5 minutes at 500 rpm with the help of a magnetic stirrer (IKA-Werke GmbH Co. KG, Staufen, Germany) and a stir bar of 40x8mm (VWR, Radnor, Pennsylvania, United States), in order to achieve an uniform particle distribution in the solution.

Samples were oxidated under a current density of 20 A/dm² for 5 minutes. The electrolyte was stirred at 500 rpm continuously in order to maintain a distribution of particles that was homogeneous. In addition, the electrolyte temperature was maintained between 3 and 8ºC thanks to the thermostatic bath connected to the electrolytic cell and it was constantly monitored by means of a sensor. The voltage-time (V-t) transients were recorded at a sampling rate of 1 Hz during the entirety of the process. After the implant modification process, samples were cleaned under tap water for 1 minute.

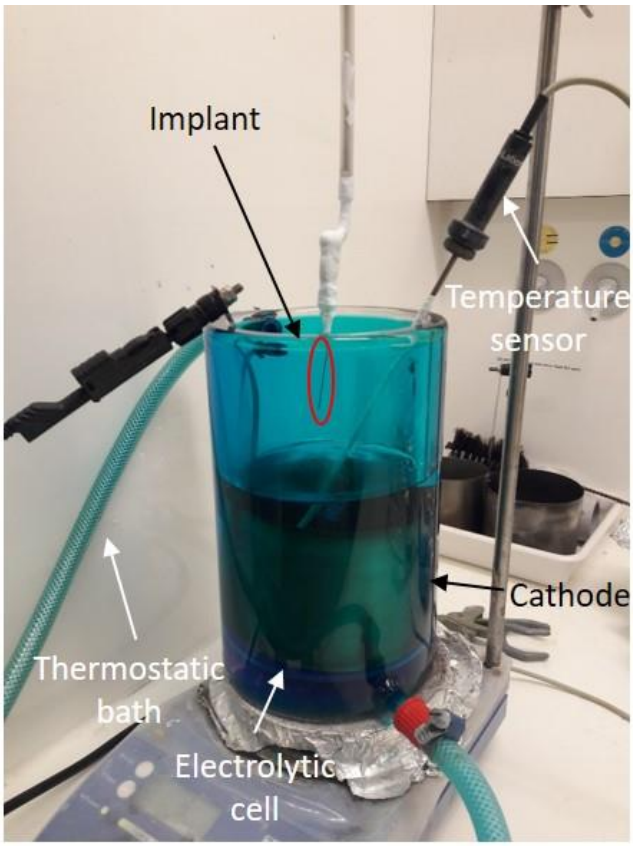

Figure 7. Overview of the electrochemical cell used for the PEO process. The double-walled cell containing the electrolyte was connected to an AC power supply through the implant that worked as anode and stainless steel cathode. The thermostatic bath kept the electrolyte cool and the temperature was monitored by a sensor.

2.3 Biomaterial characterization

2.3.1 Surface characterization

The biofunctionalized implant surface morphology was analysed using a scanning electron microscope (SEM, JSM-IT100LV, JEOL, Tokyo, Japan) with an electron beam energy ranging between 10-20 kV and 10 mm of working distance. A secondary electron detector (SED) mode was employed, which detected secondary electrons originating from the surface of the implant after previously being bombarded by an electron source. Before imaging,

samples were sputtered with a gold layer for 30 seconds in order to improve their electrical conductivity. The effects of the PEO process on the biomaterial surface morphology were observed by SEM at 50x and 500x magnifications.

2.3.2 Ion release analysis

An Inductively coupled plasma - optical emission spectrometry (ICP-OES) was used in order to measure the Ag ions released from PEO and PEO + Ag treated implants. This technique makes use of a plasma that excites the electrons of the elements present in a solution and is able to detect the characteristic wavelengths of the photons emitted by a respective element when the electrons move back to their initial energy state.

PEO and PEO + Ag implants were cut in 1cm pieces and inserted into dark Eppendorf tubes (Eppendorf, Kerkenbos, The Netherlands) with 1 ml of PBS. Tubes were placed in technical triplicates in a tube rack covered by parafilm inside a water bath and they were incubated at 37ºC. After 1 day, implants were inserted in new Eppendorf tubes with fresh PBS. These tubes corresponded to timepoint 2. This procedure was repeated for every timepoint (day 1, 2, 4, 7, 16, 21 and 28). The Eppendorf tubes with PBS collected at each timepoint were stored at 4ºC until the ion release analysis was performed. For improving the Ag ion detection, 7 ml of 3% nitric acid were pipetted to the 1ml samples at each timepoint. A control was also included which consisted of PEO only treated implants.

2.4 Cell isolation and seeding

2.4.1 Human Pediatric MSCs isolation and expansion

The isolation of human pediatric MSCs was performed from the leftover iliac crest bone chip from 3 different male donors undergoing cleft palate reconstructive surgery (ages 9-10), as previously described [42]. Cells at passages 2 or 3 were thawed and subsequently plated at 2300 cells/cm² in complete hMSC expansion medium (αMEM (Gibco, ThermoFisher Scientific, Breda, The Netherlands) supplemented with 10% v/v heat inactivated fetal bovine serum (FBS) (Sigma Aldrich, St. Louis, Missouri, USA, lot #BCCD0778), 50 µg/mL gentamycin, 1.5 µg/mL Amphothericin B, 25 µg/mL L-ascorbic acid 2-phosphate (Sigma Aldrich, St. Louis, Missouri) and 1 ng/mL fibroblast growth factor-2 (FGF_2) (Instruchemie, Delfzijl, The Netherlands)). Cells were expanded at 37ºC and 5% carbon dioxide (CO_2) in a humidified atmosphere until reaching 80-90% confluency.

2.4.2 Human Pediatric MSCs seeding on implant surfaces

PEO and PEO + Ag implants were cut in 1 cm pieces and steam sterilized at 121ºC for 90 minutes by means of an autoclave. Under sterile conditions, each implant was placed in 0.2 ml tubes (BIOplastics, Landgraaf, The Netherlands). Cells were lifted out of the culture flask via trypsinization and were seeded at a density of $1.5x10^5$ human hMSCs in 100 µl complete MSC expansion medium in the tubes containing the implants. They were incubated at 37ºC for 2 hours, while rotating them 180º every 30 minutes, in order to ensure that cells adhered evenly to the whole implant surface area. After the incubation, fresh 500 µl complete MSC expansion medium was placed in a 24 non-treated well plate (ThermoFisher Scientific, Denmark) and implants were transferred there using sterilized tweezers.

2.4.3 Human CD14+ monocyte isolation from buffy coat

The isolation of human CD14+ monocytes from buffy coats was performed by means of Ficoll (Ficoll-PaqueTM PLUS, GE Healthcare, Little Chalfont, UK) density gradient

separation and CD14+ magnetic-activated cell sorting (MACS). The Sanquin Blood bank (Sanquin blood bank, Amsterdam, The Netherlands; contract number: NVT0053.01) provided the buffy coats from the 3 different male donors for this study.

The buffy coats were transferred from the blood bag to a T175 flask (Flacon, St. Louis, USA) and were diluted with wash buffer which contained phosphate buffered saline (PBS) (Gibco, ThermoFisher Scientific, Waltham, Massachusetts, USA) and 0.1% w/v bovine serum albumina (BSA) (Sigma Aldrich, St. Louis, Missouri, USA) until the end volume was 240 ml. After the first centrifugation for 10 minutes at 220 g, the upper 15 ml layer of every 40 ml tube was removed, which contained the thrombocytes. The remaining blood was further diluted with wash buffer and 240 ml of solution was obtained. The diluted blood was separated into eight 50 ml tubes with 15 ml Ficoll solution. Each tube was slowly filled with 30 ml of blood, while keeping them at < 30º angle in order to avoid the mixing of the blood with the Ficoll.

Density gradient separation was performed by spinning the tubes at 1000 g with no brake for 15 minutes. This method takes advantage of the different density of blood cells in the sample [43]. During centrifugation, cells are separated in the solution in different layers based on the difference in their density/sizes (Figure 8). Due to their lower density, peripheral blood mononuclear cells (PBMCs) can be found in the interphase between Ficoll and plasma. The Ficoll/plasma interphases were isolated and repeatedly centrifuged for 10 minutes at 800 x g, while collecting the supernatants in between. The process was repeated until no supernatant was visible anymore. Pellets were diluted with PBS, containing 0.5% w/v BSA and 2mM EDTA (Invitrogen, Carlsbad, California, USA) and any possible clumps were removed by filtering them through a 30 µm filter.

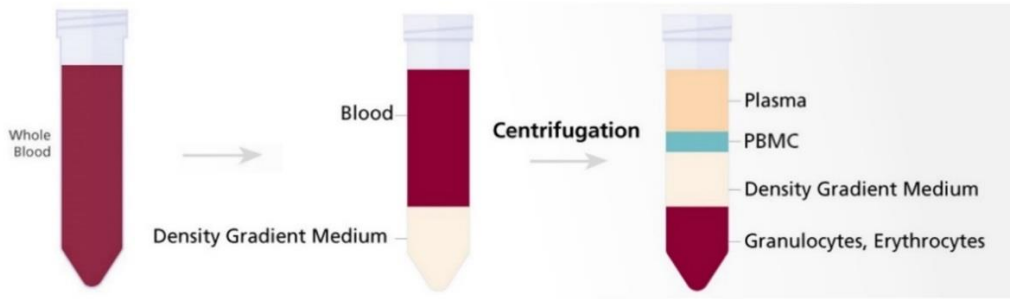

Figure 8. Schematic overview of the different steps involved in the density gradient separation process. After thrombocyte removal, a density gradient medium is added to blood samples. Following centrifugation, cells are separated in the solution in layers based on the difference in their density/sizes. Image adapted from [44].

Monocyte isolation was performed by first labelling PBMCs with 100 µl of anti-CD14+ magnetic bead solution (Miltenyi Biotec, Bergisch Gladbach, Germany) by incubating them at 4ºC and in the dark for a period of 20 minutes. Subsequently, the cell suspension was applied to a CD14 + magnetic-activated cell sorting (MACS) (Miltenyi Biotec, Bergisch Gladbach, Germany). Monocytes are known to have high expressions of the CD14 cell surface receptor. When the CD14+ labelled cell suspension is applied to a MACS column and magnet, the strong magnetic field captures those cells that have an anti-CD14+ bead attached to them, which correspond to those cells that possess the CD14 surface marker.

2.4.4 Human monocyte seeding on implant surfaces

PEO and PEO + Ag implants were cut in 1 cm pieces and steam sterilized at 121ºC for 90 minutes by means of an autoclave. Under sterile conditions, each implant was placed in 0.2 ml tubes (BIOplastics, Landgraaf, The Netherlands) and was seeded with $5x10^5$ human CD14+ monocytes in 100 µl X-vivo 15 medium (Lonza Group GA, Basel, Switzerland) supplemented with 20% v/v heat inactivated FBS, 50 mg/ml gentamycin and 1.5 mg/ml Amphothericin B. The implants were incubated at 37ºC for 2 hours, while rotating them 180º every 30 minutes, in order to ensure that cells adhered evenly to the whole implant surface area (Figure 9). After the incubation, fresh 400 µl of X-vivo medium was placed in another 48-well plate and implants were transferred there by means of sterilized tweezers.

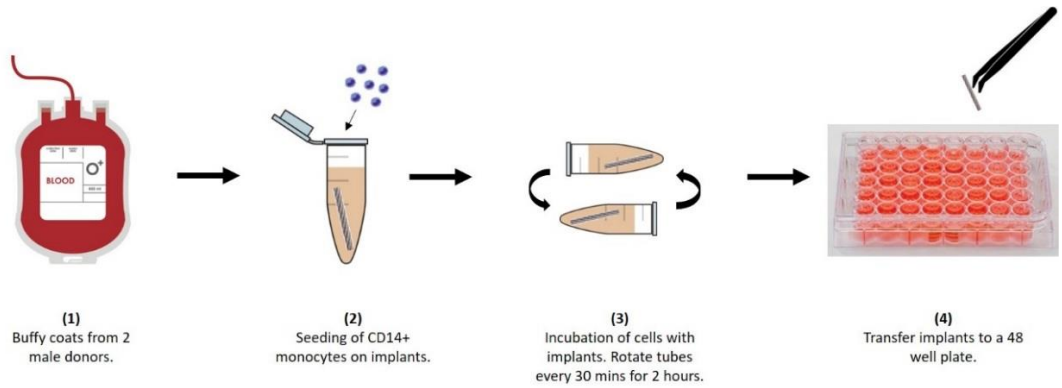

Figure 9. Schematic overview of the experimental setup for CD14+ monocyte seeding on the implants.

2.5 *In vitro* osteogenic evaluation of hMSCs cultured on PEO biofunctionalized implants

The hMSCs were cultured on the implants in order to evaluate the effects of the PEO-modified surfaces on the osteogenic activity of the cells. Cell extracellular matrix (ECM) calcification and morphology and osteogenic gene expression levels were investigated.

2.5.1 ECM mineralization

2.5.1.1 Calcium concentration in culture medium

The process of osteogenic differentiation of hMSCs can be monitored by measuring the calcium concentration in the medium at various timepoints. Osteogenically differentiating hMSCs are characterized by taking up calcium from the medium to start the mineralization of their matrices, forming calcium deposits. The calcium uptake assay is a colorimetric assay based on the reaction of calcium with o-cresophthalein complexone in an alkaline solution. When the Ca^{2+}-o-cresophthalein complex is formed, the color of the medium changes from a light brown-greyish to a bright purple-pink colored complex. The calcium concentration present in the sample is proportional to the intensity of the pink-purple color formed and can be measured with a spectrophotometer at 570 nm.

Following 24 hours of culture in complete expansion medium, three 1 cm implants were transferred per well in technical triplicates and per experimental group to a 24 non-treated well-plate containing 250 µl of osteogenic induction medium (high-glucose DMEM

(Gibco, ThermoFisher Scientific, Breda, The Netherlands) supplemented with 10% v/v heat inactivated FBS, 50 µg/mL gentamycin, 1.5 µg/mL Amphothericin B and fresh 0.1 µM dexamethasone, 0.1 mM L-ascorbic acid 2-phosphate and 10 mM β-glycerophosphate (Sigma-Aldrich, St. Louis, Missouri, USA)). Cells were cultured at 37ºC and 5% CO_2 and the medium was refreshed every 3-4 days. Control wells were also included, consisting of implants with no cells and were also cultured in osteogenic induction medium.

200 µl of cell culture supernatant was collected at timepoints 3, 7, 10, 14, 17, 21 and 24 days and stored at -20ºC until the calcium assay was performed. Implants were moved to another well plate at day 14 in order to avoid the interference of cells detached from the implants. An eight-point standard curve was made with calcium chloride ($CaCl_2$) in a concentration range of 0-3 mM in calcium free αMEM (Gibco, ThermoFisher Scientific, Breda, The Netherlands, catalogue n. # 041-91867M, lot #2283388) and those known values were used in order to calculate the calcium concentration present in each sample. 10 µl of sample were mixed with 100 µl of calcium reagent (1+1 mix of 1 M ethanolamine pH 10.5 and 0.35 mM o-cresophthalein complexone, 19.8 mM 8-hydroxyquinoline and 0.6 M hydrochloric acid, all from Sigma-Aldrich, St. Louis, Missouri, USA)) and the optical density of each sample was determined by a VersaMax spectrophotometer (Molecular Devices, San Jose, California, USA) at a wavelength of 570 nm.

2.5.1.2 Xylenol orange labelling

The mineralization of the ECM of osteogenically differentiating cells can be visualized by a xylenol orange labelling. This fluorochrome is known to bind to newly formed calcified tissues and can be analyzed by a fluorescence source [45].

Xylenol orange tetrasodium salt (Honeywell Research Chemicals, Charlotte, US) was added in a concentration of 20 µM after 3 days of medium switch to osteogenic induction medium and in every medium refreshment. At day 31 images of the live cells were taken using a confocal microscope (ZEISS LSM 510 Meta inverted confocal microscope, Zeiss, Cologne, Germany). A control was also included which consisted of implants cultured in xylenol orange but with no cells.

2.5.1.3 ECM morphology

The morphology of the mineralized ECM of cells was observed by SEM (JSM-IT100LV, JEOL, Tokyo, Japan). After culturing them for 24 days, cells were rinsed in PBS and then fixed with 4% w/v paraformaldehyde (PFA) and 1% v/v glutaraldehyde in PBS for two hours at 4ºC. Then, cells were dehydrated gradually in increasing ethanol solutions (50, 70 and 96%) and were dried in an Eppendorf tube (Eppendorf, Hamburg, Germany) for at least two hours. The samples were mounted on an aluminium stub with a carbon sticker and were gold sputtered for 1 minute in order to enhance their electrical conductivity. Images were taken at SED mode at 50x and 500x magnifications.

2.5.2 Gene expression analysis

The osteogenic gene expression levels of osteogenically differentiated hMSCs were assessed by a reverse transcription quantitative polymerase chain reaction (RT-qPCR). This technique comprises three steps: mRNA isolation, reverse transcription (RT) for complementary DNA (cDNA) synthesis and quantitative polymerase chain reaction (qPCR).

2.5.2.1 RNA isolation

Cells were harvested at day 7 of osteogenic differentiation and lysed by the addition of 400 µl RNA STAT-60 (Tel-Test, Friendswood, Texas, US). RNA STAT-60 disrupts the cells but maintains the RNA integrity by inhibiting the RNAse activity. Samples were collected and

stored at -80ºC until the mRNA isolation was performed (Figure 10). First, a phase separation was performed by adding 80 µl of chloroform to each sample and centrifuging them for 15 minutes at 12.000 g. RNA could be found in the aqueous phase of the tube, which was collected and an equal volume of 70% v/v ethanol was added. This solution was loaded in a RNeasy micro column (Qiagen, Germantown, USA) and centrifuged for 30 seconds at 8.000 g. RNA is precipitated onto the RNeasy column in this step. Next, salts were removed from the medium by adding 350 µl buffer RW1 (guanidine salts and ethanol) and centrifuging columns for 30 seconds at 8.000 g. Residual genomic DNAse was removed by adding 75 µl of DNAse buffer (10 µl DNAse (Qiagen, Germantown, USA, supplied with kit) and 70µl buffer RDD per sample). After 15 minutes of incubation at room temperature, DNAse and residual salts were further removed by addition of 350 µl buffer RW1, 500 µl of RPE and 500 µl 80% v/v ethanol and centrifuging 30 seconds at 8.000 g in between the addition of each reagent. After the last wash, the columns were centrifuged with open caps for another 5 minutes at 8.000 g to ensure that columns were dry, and all traces of ethanol were removed. RNA was eluted from the columns in 16 µl of RNAse free ddH_2O. Following 1 minute of incubation, a 1 minute centrifugation of the columns was performed at 8.000 g. This last step unbinds the isolated RNA from the RNeasy column, transferring the freshly isolated RNA to a 1.5 ml tube. Finally, the total isolated RNA was quantified by means of a spectrophotometer/fluorometer (DSS-11 Series Spectrophotometer/fluorometer, DeNovic, Wilmington, USA) at 260/280 nm.

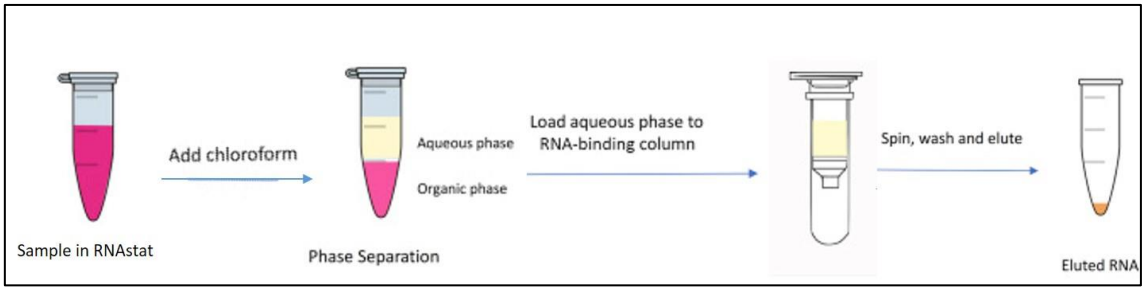

Figure 10. Schematic overview of the different steps involved in the RNA isolation process using a RNeasy micro column.

2.5.2.2 cDNA synthesis

After RNA quantification, a two-step RT-qPCR approach was followed (Figure 11) to obtain the gene expression of differentiating hMSCs. Firstly, cDNA was synthesized via RT process, in which a reverse transcriptase enzyme creates the complementary DNA from the isolated RNA samples. The RevertAid First Strand cDNA Synthesis Kit (Thermo Fischer Scientific, Waltham, Massachusetts, USA) was used to perform the synthesis, following the manufacturer's instructions. Briefly, the previously isolated RNA was incubated with 0.5 µl of Oligo-d(T)18 primer, 0.5 µl Random Hexamer primer and ddH_2O for 5 minutes at 70ºC. The volume of sample taken depended on the concentration of RNA present in each sample and the added amount of water was adjusted in each case to obtain 12 µl of final volume. After keeping the samples at 5 minutes in ice, the enzyme mix containing reaction buffer, dNTPs, Ribolock inhibitor and RevertAid MMulV Reverse Transcriptase was added to each sample. Two controls were also included in the analysis: a sample without Reverse Transcriptase and a no template control, containing ddH_2O, enzymes, dNTPs and buffer, but no sample. Samples were incubated first for 5 minutes at 25ºC, then 60 minutes at 42ºC and

finally 10 minutes at 70ºC. After cooling down to 12ºC, cDNA samples were diluted by the addition of 100 µl ddH_2O to each sample.

2.5.2.3 RT-qPCR

The second step of the two-step RT-qPCR approach is to perform the qPCR to quantify the hMSCs gene expression. The gene expression level in a cell can be measured by quantifying the amount of copies of an RNA transcript of that gene. The qPCR is a technique that monitors the amplification of a cDNA sample previously obtained from an RNA sample. This technique is based on the use of fluorescent dyes and primers specific to each gene, such as TaqMan FAM/TAMRA probe or SYBR Green dye that bind to specific cDNA strands and emit increasing fluorescence as the quantity of produced DNA increases. The amount of obtained fluorescence signal is proportional to the levels of expression of a gene in a cell sample. A mastermix solution was prepared for each gene, composed of 5.0 µl of 2x qPCR mastermix (TaqMan Universal PCR mastermix (Thermofischer), or qPCR Mastermix Plus for SYBR GreenI (Eurogentec)), 0.5 µl of primer mix and 2.5 µl of ddH_2O. 8 µl of mastermix and 2 µl of cDNA were pipetted to a PCR plate and a Bio-Rad CFX96 Real-Time PCR Detection system (Bio-Rad, Hercules, CA, USA) was used to quantify the gene expression.

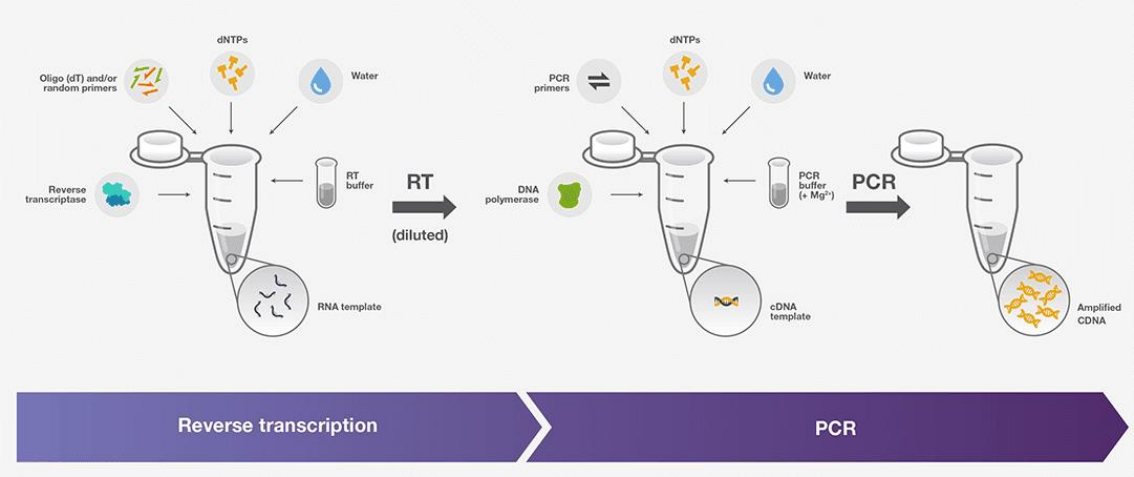

Figure 11. Schematic overview of the different steps involved in the two-step RT-qPCR assay. Image adapted from [46].

The best housekeeper index (BKI) was calculated by performing the geometric mean expression of the genes Glyceraldehyde-3-phosphate dehydrogenase (GAPDH), Beta-2-Microglobulin (B2M) and Ubiquitin C (UBC). This index allowed for the normalization of each gene expression value. The hMSCs osteogenic differentiation was studied by measuring the gene expression of certain osteogenic genes that are known to be characteristic of the osteogenic differentiation process. The full list of osteogenic genes and primers can be found in Table 1. Early and late osteogenic markers were used. The following equation was used to calculate the gene expression relative to the BKI expression: Gene Expression = $2^{-\Delta Cq}$, where ΔCq = Cq from gene of interest -Cq from BKI.

Table 1. List of early and late osteogenic markers and housekeeper genes with the corresponding primers and probes used for RT-qPCR analysis.

	Gene	Forward (5'- 3')	Reverse (5'- 3')	Probe (FAM, 5'- 3')
Early osteogenic marker	***COL-1***	CAGCCGCTTCACCTACAGC	TTTTGTATTCAATCACTGTCTTGCC	CCGGTGTGACTCGTGCAGCCATC
	RUNX2	ACGTCCCCGTCCATCCA	TGGCAGTGTCATCATCTGAAATG	ACTGGGCTTCTTGCCATCACCGA
Late osteogenic marker	***ALPL***	GACCCTTGACCCCCACAAT	GCTCGTACTGCATGTCCCCT	TGGACTACCTATTGGGTCTCTTCGAGCCA
	IBSP	TGCCTTGAGCCTGCTTCC	GCAAAATTAAAGCAGTCTTCATTTTG	CTCCAGGACTGCCAGAGGAAGCAATCA
Housekeepers	***GAPDH***	ATGGGGAAGGTGAAGGTCG	TAAAAGCAGCCCTGGTGACC	CGCCCAATACGACCAAATCCGTTGAC
	B2M	TGCTCGCGCTACTCTCTCTTT	TCTGCTGGATGACGTGAGTAAAC	
	UBC	ATTTGGGTCGCGGTTCTTG	TGCCTTGACATTCTCGATGGT	

2.6 In vitro interactions between hMSCs and macrophages

In order to investigate the effect of macrophage polarization induced by PEO/PEO + Ag implants on hMSCs osteogenic differentiation via paracrine communication an indirect co-culture model was developed in this study. The development of the model is presented in the following sections.

2.6.1 hMSCs and macrophages indirect co-culture

hMSCs were isolated and seeded on various samples as explained in sections 2.4.1 and 2.4.2 for 24 hours in expansion medium. Monocytes were seeded on various samples as explained in sections 2.4.3 and 2.4.4 and were cultured in X-vivo medium for 48 hours. After that time, both types of cells on the implants were placed together in a non-treated 12 well plate in 800 µl of co-culturing medium (high-glucose DMEM (Gibco, ThermoFisher Scientific, Breda, The Netherlands) supplemented with heat inactivated 10% v/v FBS, 50 µg/mL gentamycin, 1.5 µg/mL Amphothericin B and fresh 0.1mM L-ascorbic acid 2-phosphate (Sigma-Aldrich, St. Louis, Missouri, USA)). For each cell type, seeded implants were placed in every well in triplicates and a separating line was formed with 0.5 ml of 2% w/v agarose in the middle of the well to avoid any possible direct contact between the two different types of cells. However, both cells shared the same medium. After three days of co-culture, the implants with hMSCs and macrophages were separated for further immunological and osteogenic evaluations. Figure 12 shows the steps involved in the setting up of the co-culture.

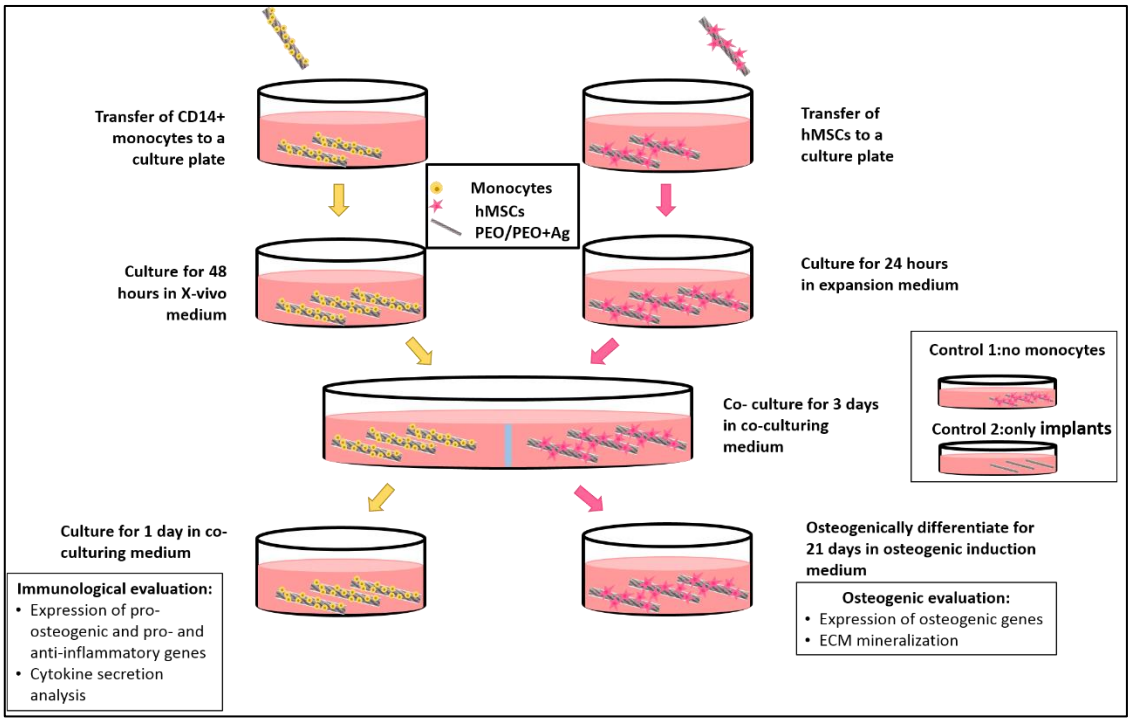

Figure 12. Schematic diagram of the hMSCs and macrophage indirect co-culture setup.

2.6.2 Immunological evaluation of macrophages in co-culture

2.6.2.1 Gene expression analysis

Macrophages were harvested after 3 days of co-culture and the expression of pro-osteogenic, pro- and anti-inflammatory and tissue-repair genes were assessed by means of a reverse transcription quantitative polymerase chain reaction (RT-qPCR) as explained previously in section 2.5.2. The full list of genes and primers used for this evaluation are listed in Table 2.

Table 2. List of pro- and anti- inflammatory, tissue-repair, pro-osteogenic and housekeeper genes with the corresponding primers and probes used for RT-qPCR analysis.

	Gene	Forward (5'- 3')	Reverse (5'- 3')	Probe
Pro-inflammatory	***IL-6***	TCGAGCCCACCGGGAACGAA	GCAGGGAAGGCAGCAGGCAA	
Tissue-repair	***CCL18***	GCACCATGGCCCTCTGCTCC	GGGCACTGGGGGCTGGTTTC	
Anti-inflammatory	***CD163***	GCGGGAGAGTGGAAGTGAAAG	GTTACAAATCACAGAGACCGCT	
Pro-osteogenic	***OSM***	GACGCTGCTCAGTCTGGTCC	AGCACGCGGTACTCTTTCG	
	BMP2	TaqMan assay on demand: Hs00154192_m1 (Applied Biosystems, Foster city, CA, USA)		
	PTGS2	TaqMan assay on demand: Hs00153133_m1 (Applied Biosystems, Foster city, CA, USA)		
Housekeepers	***GAPDH***	ATGGGGAAGGTGAAGGTCG	TAAAAGCAGCCCTGGTGACC	CGCCCAATACGACCAAATCCGTTGAC
	B2M	TGCTCGCGCTACTCTCTCTTT	TCTGCTGGATGACGTGAGTAAAC	
	UBC	ATTTGGGTCGCGGTTCTTG	TGCCTTGACATTCTCGATGGT	

2.6.2.2 Protein secretion analysis

An enzyme-linked immunosorbent assay (ELISA) was employed to study the macrophage polarization pattern that happened during the co-culture with hMSCs. This can be achieved by analyzing the macrophage secretion levels of different factors. More specifically, in this study the secretion levels of the pro-inflammatory cytokine IL-6, characteristic of M1 proinflammatory macrophages, and the tissue repair-related chemokine CCL18, characteristic of M2a anti-inflammatory macrophages released in the supernatant were evaluated.

After 3 days of co-culture, macrophages were transferred to a non-adherent 24 well plate with 500 µl co-culturing medium and 24 hours later 400 µl of cell supernatant was collected and stored at -80ºC in 1.5 ml tubes (Eppendorf, Hamburg, Germany) until the analysis was performed. Commercially available ELISA kits were employed (DuoSet Development Kit; RD Systems, Mckinley, Minneapolis, USA), which used the sandwich ELISA method (Figure 13). Firstly, 100 µl of capture antibody was pipetted into a 96-well plate and were incubated overnight at room temperature. The next day, each well was washed three times with 400 µl of wash buffer which contained PBS and 0.5% v/v Tween (Sigma-Aldrich, St. Louis, Missouri, USA) in order to remove residual unbound antibodies. The addition of 300 µl reagent diluent composed of 10% v/v reagent diluent concentrate (RD Systems, Mckinley, Minneapolis, USA) to each well ensured that any remaining protein-binding sites on the plate was blocked. After 1 hour of incubation at room temperature, the washing was repeated. Then, 100 µl of sample or standards were pipetted in duplicates. After 2 hours of incubation and subsequent washing of plates, 100 µl of biotin labelled detection antibody was added to each well, which binds to any antigen present in the well. Following another 2 hours of incubation and subsequent washing of plates, 100 µl of streptavidin-HRP solution was pipetted and the plate was incubated avoiding light exposure during 20 minutes at room temperature. After a final wash and incubation with 100 µl of substrate solution (1 H_2O_2: 1 tetramethylbenzidine (TMB), supplied with the kit) for 20 minutes, 50 µl of stop solution (2N H_2SO_4) was pipetted to the wells. The substrate solution is converted by streptavidin-HRP to a colored product in proportion to the amount of analyte present in the sample. Finally, a Spectramax ID3 (Molecular Devices, San Jose, California, USA) at a wavelength of 450 nm and 540 nm was used to determine the optical density of each well.

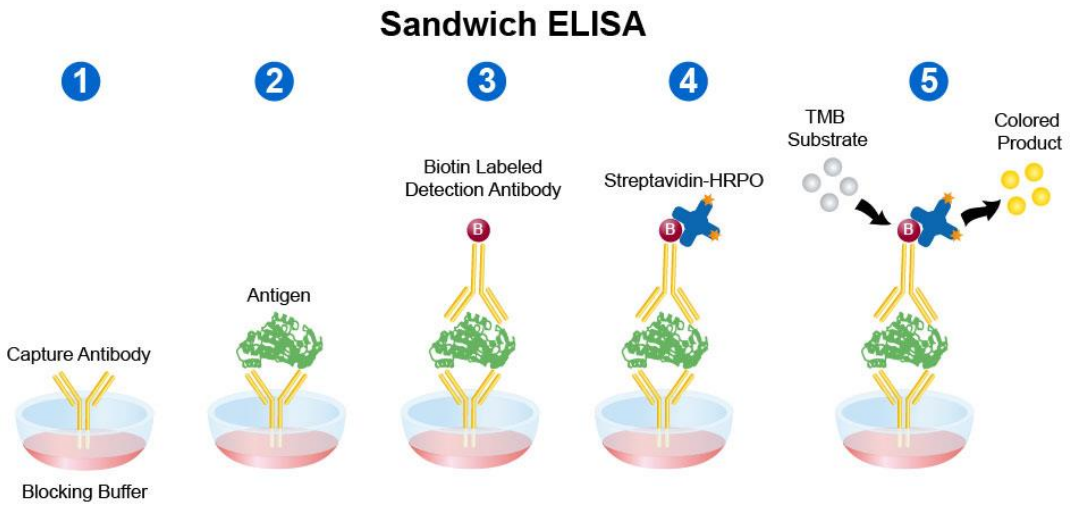

Figure 13. Schematic overview of the different steps involved in the sandwich ELISA assay [47]. (1) A layer of capture antibodies is formed in the bottom of the wells and the blocking buffer blocks any remaining protein-binding site. (2) Any targeted antigen in the sample binds to the capture antibody. (3) A biotin labelled detection antibody binds to the antigens, forming the "sandwich". (4) The enzyme streptavidin-HRP complex is bound to the detection antibody. (5) The TMB substrate solution is transformed onto a colored product by the antibody streptavidin-HRP complex.

2.6.2.3 DNA quantification

The DNA content of macrophages incubated with implants was quantified after 3 days of co-culture and 1 day of single-culture. The quantification was performed to measure the number of cells that managed to bind to each surface type as well as to normalize the protein content in the culture media measured with ELISA. This allows for the adjustment of the variation in cell number and for the determination of the amount of cytokines produced per cell.

Implants with adhered macrophages were harvested and stored at -80ºC in 1.5 ml tubes (Eppendorf, Hamburg, Germany). The DNA quantification was performed by the use of a CYQUANT cell proliferation assay (Invitrogen, Carlsbad, California, USA). Firstly, cells attached to the biomaterials were lysed and digested for 16 hours at 60ºC in 200 µl papain digestion solution, composed of 250 µg/ml Papain and 0.01 M Cysteine-HCL (Sigma Aldrich, San Luis, Missouri, USA) in 0.2 M NaH_2PO_4 and 0.01 M EDTA.$2H_2O$, pH 6.0. Next, a 96-well plate was filled with either 50 µl samples or standard in duplicate. 250 µl IU heparin solution and 125 µl of ribonuclease type 3 were added to each well to remove RNA from the samples, which is also able to bind to the dye and can give a false signal. After incubating the samples for 30 minutes at 37ºC, 0.375 µl of CYQUANT GR dye was pipetted to each well. This fluorescent die strongly increases its signal when bound to nucleic acids [48]. Finally, the fluorescence value of each well was determined on a Spectramax ID3 (Molecular Devices, San Jose, California, USA) at a wavelength of 480 nm for the excitation and 520 nm for the emission.

2.6.3 Osteogenic evaluation of hMSCs in co-culture

2.6.3.1 ECM mineralization: calcium concentration in culture medium

After 3 days of co-culture, three 1 cm implants with hMSCs were transferred to a 24 non-adherent well plate per well with 250 µl of osteogenic induction medium and were cultured for 21 days. 200µl of cell culture supernatant was collected at timepoints 3, 7, 10, 14, 17 and 21 days and a calcium assay was performed as previously explained in section 2.5.1.1.

2.6.3.2 Gene expression analysis

Co-cultured hMSCs were further cultured in a non-adherent 24 well plate with 250 µl of osteogenic induction medium for another 7 days, then they were harvested. The expression of osteogenic genes was assessed by means of the RT-qPCR technique as explained previously in section 2.5.2. The full list of osteogenic genes and primers can be found in Table 1.

2.7 Statistical analysis

IBM SPSS 25.0 was employed for the statistical evaluation in this study. The figures portray mean value +- standard deviation. The Kolmogorov-Smirnov test was used to test the normal distribution of the data. Then, a linear mixed model was used followed by the Bonferroni *post-hoc* test. The different implant conditions were considered as fixed factors and the donors as random factors.

3. RESULTS

3.1 Implant characteristics

PEO treatment of the AM implants modified the surface morphology through the creation of a thick titanium oxide layer and interconnected micro- and nano-porous structures (Figure 14. A, B). The incorporation of AgNPs did not change the topographical features of the surfaces (Figure 14. C, D). In addition, similar voltage transients were observed for both types of implants (Figure S1).

The incorporation of AgNPs into the PEO + Ag implant surfaces was confirmed through the analysis of Ag ion release pattern in PBS (Figure 14. E). A constant increase of the total ion concentration was observed, reaching to a cumulative value of over 800 ppb at day 28.

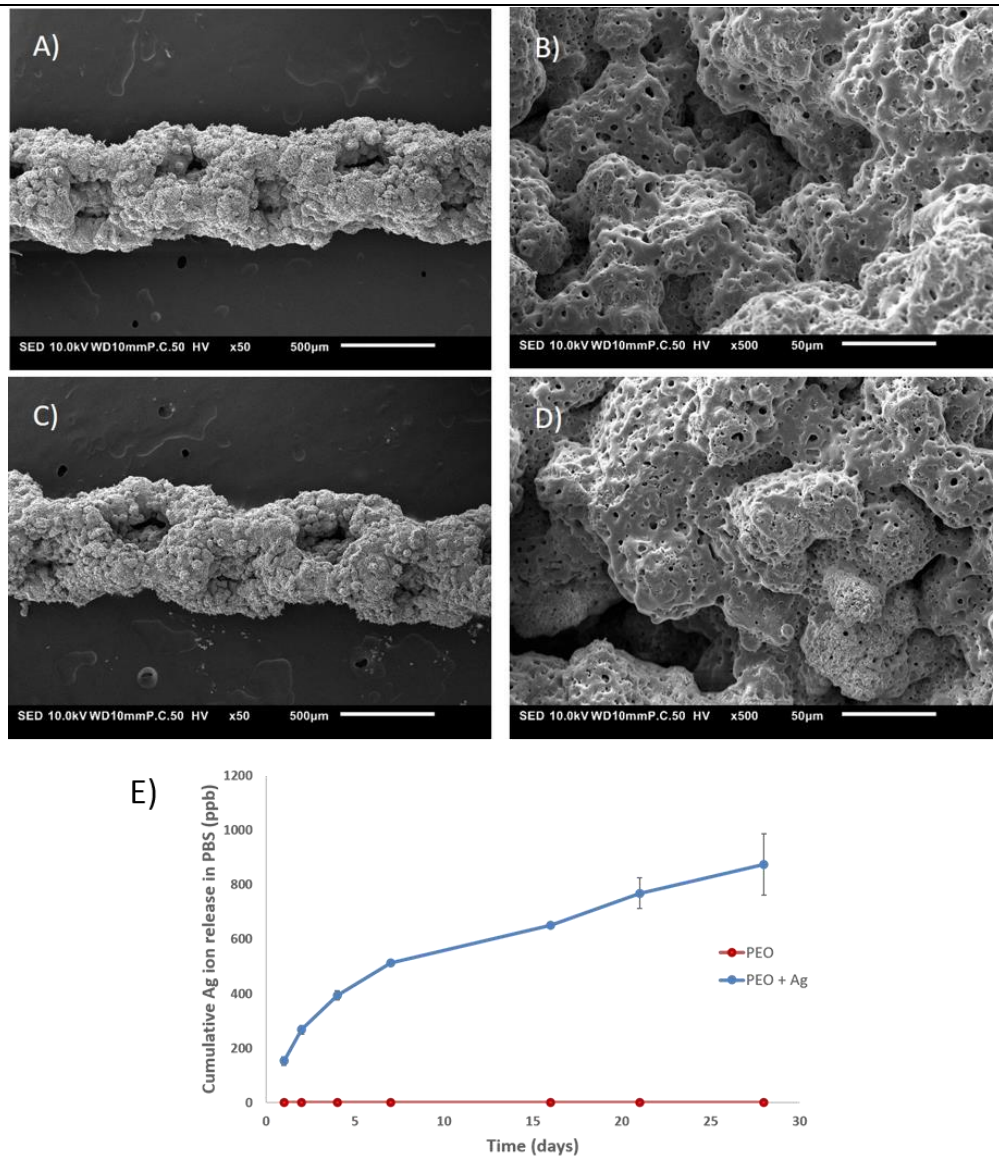

Figure 14. Surface characterisation. (A,B) SEM images showing the characteristic surface morphology of the PEO-modified AM implants. (C,D) SEM images of the PEO + Ag implants. (E) Cumulative Ag ion release pattern in PBS over a period of 28 days.

3.2 Osteogenic evaluation of hMSCs attached to implant surfaces

hMSCs originating from 3 different donors were cultured with PEO/PEO + Ag surfaces in a monoculture and their osteogenic activity was evaluated.

hMSCs cultured on implant surfaces significantly increased their calcium uptake from day 14 onwards compared to day 3 as evidenced by a 0.2 relative decrease in the concentration of Ca^{2+} in the culture medium (Figure 15. A). No significant differences were observed between PEO and PEO + Ag implants. In addition, after day 10 Ca^{2+} levels in culture medium in controls (i.e. implants cultured in the absence of cells) were significantly higher than for implants cultured with cells suggesting that free Ca^{2+} ions present in the medium did not show a tendency to attach to the bare biomaterials (Figure S2).

hMSC mineralization was further investigated by a xylenol orange labelling of newly forming calcium deposits. Confocal images detected a positive signal for calcium on the hMSCs cultured on both PEO and PEO + Ag groups at day 31 of culture, but not on the control group (i.e., implants cultured with xylenol orange in the absence of cells) (Figure 15. B).

Morphology of mineralized ECM of cells was visualized by SEM imaging at day 24 revealing the ability of the cells to completely cover the implants and produce an abundance of matrix (Figure 15. C). Interestingly, very fine structures of ca. 0.5-1 µm were observed at 2000x magnification, suggesting the presence of collagen fibers, characteristic for the ECM of MSCs (Figure 15. C3).

Another analysis of the osteogenic commitment of MSCs was gene expression. The results showed that the expression levels of selected genes related to osteogenesis (*COL1*, *RUNX2*, *ALPL* and *IBSP*) were comparable on hMSCs cultured on both PEO and PEO + Ag implants at day 7 of the culture (Figure 16). Their Cq values can be found in Table S1.

Taken together, these findings suggest that hMSCs are able to osteogenically differentiate and mineralize when seeded on the PEO and PEO + Ag implants. The presence of AgNPs on the implants proved not to compromise the osteogenesis process.

3.3 Immunological response of co-cultured macrophages

An indirect macrophage/hMSC co-culture model was developed in this study. Firstly, macrophage polarization state induced by PEO/PEO + Ag implants was investigated.

DNA content of human monocyte-derived macrophages was significantly higher ($p \leq 0.05$) on PEO + Ag implants after 3 days of co-culture and 1 day of single-culture (Figure 17. A). ELISA measurement of proteins secreted by co-cultured macrophages after 1 day of single-culture indicated similar levels of the pro-inflammatory cytokine IL6 and tissue-repair chemokine CCL18 in both PEO and PEO + Ag groups (Figure 17. B, D). However, normalization of cytokine levels with the DNA content revealed that PEO treated implants induced a higher secretion of CCL18 per cell ($p \leq 0.0001$) (Figure 17. C). Normalized Il6 levels were comparable between PEO and PEO + Ag groups (Figure 17. E).

Following the same tendency to normalized protein secretion levels, the pro-inflammatory gene *IL6* was similarly expressed in both specimens after 3 days of co-culture (Figure 18. A) whereas the tissue-repair gene *CCL18* was significantly more expressed in

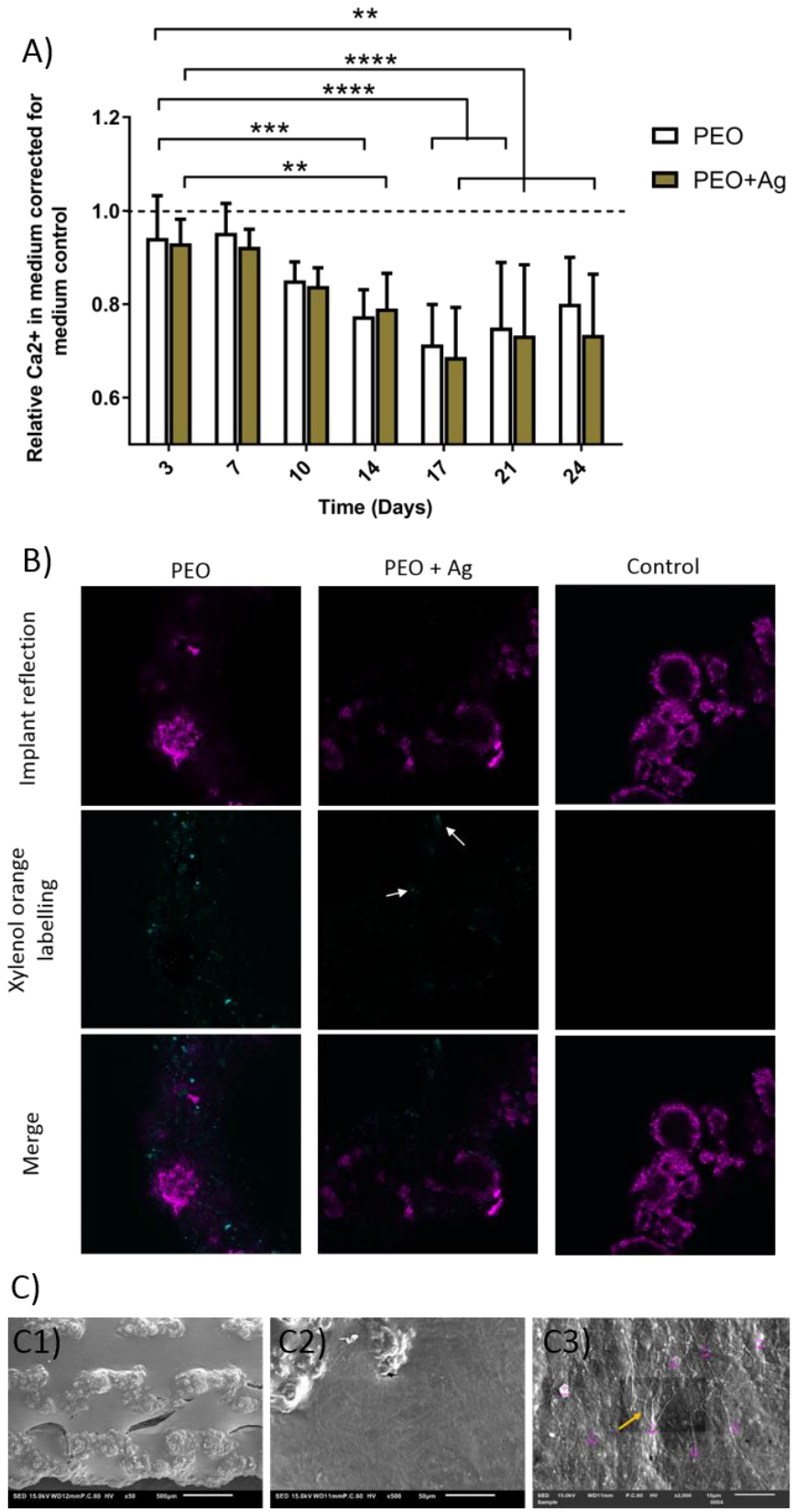

Figure 15. ECM mineralization of hMSCs cultured on implant surfaces. (A) Relative Ca^{2+} concentration in culture medium for hMSCs cultured on PEO and PEO + Ag implants over a period of 24 days. $p \leq 0.01$ (**), $p \leq 0.001$ (***), $p \leq 0.0001$ (****). (B) Confocal images of xylenol orange labelling (cyan) for hMSCs cultured on PEO and PEO + Ag implants (magenta) for 31 days. (C) SEM images of the ECM produced by hMSCs on the implant surfaces after 24 days of culture.

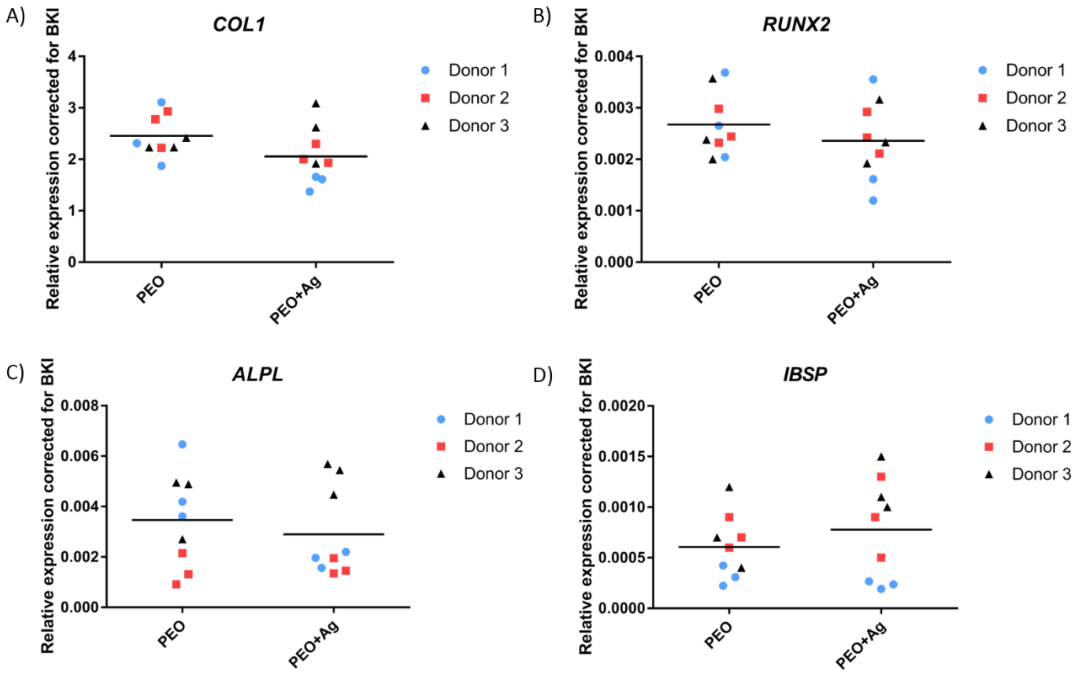

Figure 16. Osteogenesis of hMSCs cultured on implants surfaces. Gene expression levels of osteogenesis-related genes in hMSCs cultured on PEO and PEO+Ag implants after 7 days of culture.

PEO surfaces ($p \leq 0.01$) compared to PEO + Ag implants (Figure 18. B). Similarly, levels of surface marker *CD163* expressed by anti-inflammatory M2 type macrophages were significantly higher in PEO treated implants (Figure 18. C) ($p \leq 0.001$). In the case of pro-osteogenic genes (*OSM*, *PTGS2* and *BMP2*), two out of three genes were detectable in both implant types. This trend was followed by all three donors. Comparable expression levels of *OSM* and *PTGS2* were measured in PEO and PEO + Ag implants (Figure 18. D, E), whereas *BMP2* was undetectable. Their Cq values can be found in Table S2.

Summarizing, the analysis of the co-culture immune response revealed that PEO surfaces have a tendency towards a higher pro-repair gene expression and protein secretion compared to PEO + Ag implants. By comparison, no differences in the pro-inflammatory and pro-osteogenic response were observed between the two groups.

3.4 Osteogenic response of co-cultured hMSCs

Secondly, the indirect co-culture allowed to study the paracrine effect of the macrophage response to implants on the osteogenic activity of hMSCs.

Co-cultured hMSCs caused a significant drop in the Ca^{2+} concentration in the culture media from day 10 onwards comparing to day 3 on both PEO and PEO + Ag surfaces (Figure 19). No differences were observed between the two types of implants.

As previously observed in section 3.2, osteogenesis-promoting genes (*COL1*, *RUNX2*, *ALPL* and *IBSP*) were similarly expressed on hMSCs cultured on both PEO and PEO + Ag implants after 3 days of co-culture and 7 days of single monoculture in osteogenic induction medium. In addition, no gene expression differences were observed between the single- or co-cultured hMSCs on neither specimens (Figure 20). This tendency was consistent for all donors. Their Cq values can be found in Table S3.

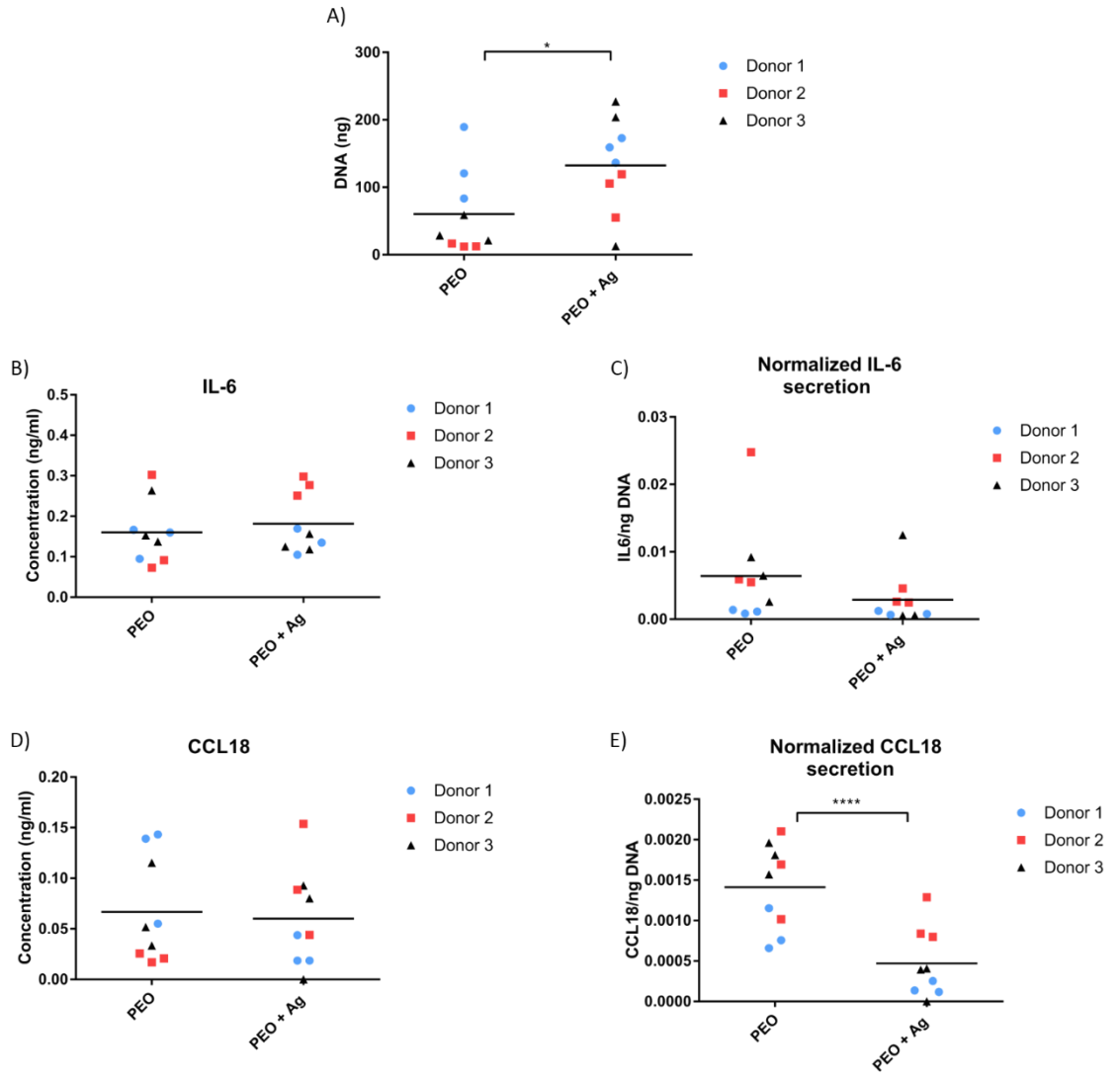

Figure 17. DNA and proteins secreted by co-cultured human monocyte-derived macrophages attached to implant surfaces after 3 days of co-culture and 1 day of single-culture in co-culturing media. (A) DNA quantification. (B, D) ELISA measurements of the concentration of IL6 and CCL18 in culture media. (C, E) Normalized values of IL6 and CCL18 secretion to DNA. $p \leq 0.05$ (*), $p \leq 0.0001$ (****).

4. DISCUSSION

The clinical success of orthopedic implants relies on the minimization of implant failures. Biomaterial fabrication and modification strategies have currently a significant focus on the favorable outcome of these structures by enhancing their bioactivity including the osteoimmunomodulatory properties. One such promising structure was developed by our team in a previous study consisting of Ti-6Al-4V structures developed with AM and biofunctionalized by PEO and the incorporation of AgNPs [34]. The aim of this strategy was to achieve dual osseointegration and antibacterial functionalities. Their results showed high antibacterial activity of Ag-incorporated implants against methicillin-resistant *Staphylococcus aureus* (MRSA) and no cytotoxic effects on hMSCs. However, considering the importance of the immune system in the acceptance of the biomaterial by the body and in

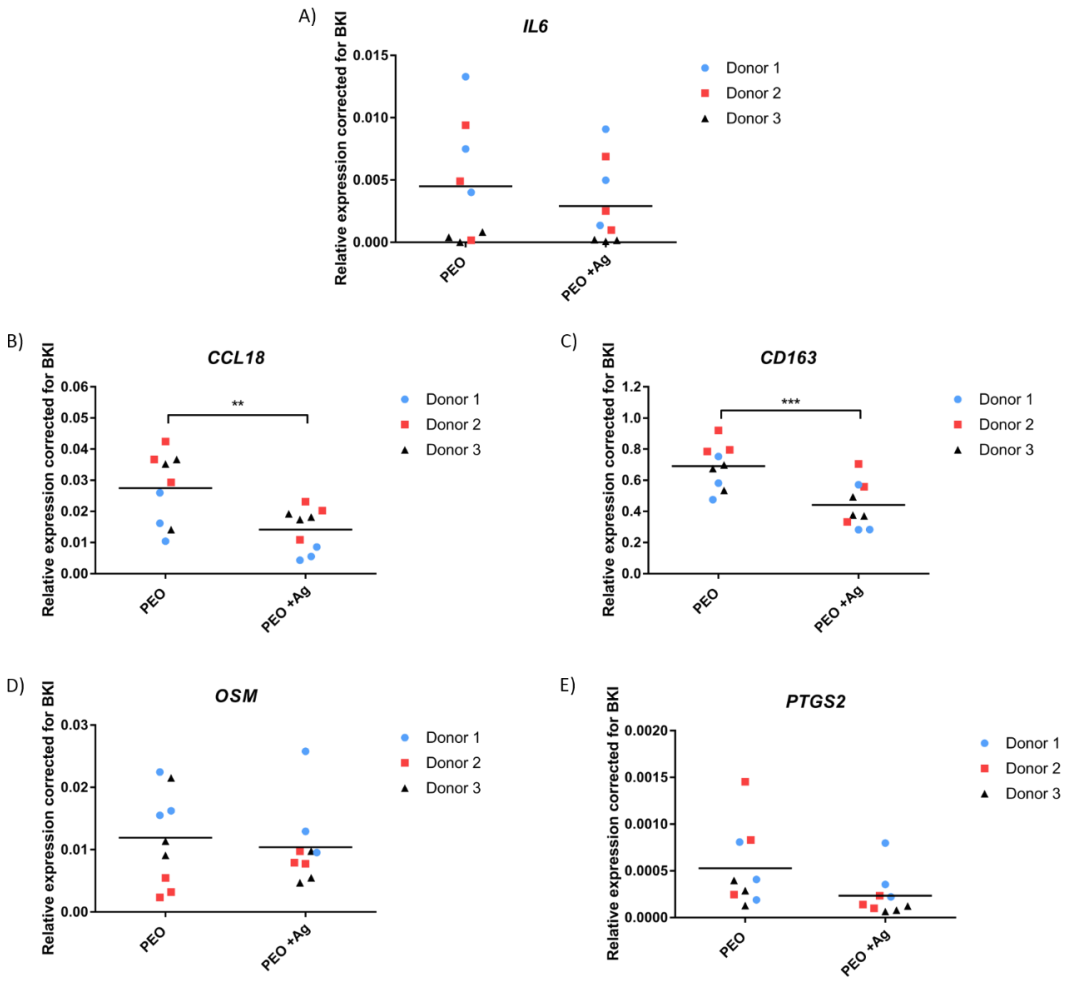

Figure 18. Gene expression levels of co-cultured human monocyte-derived macrophages attached to implant surfaces on day 3 of co-culture. $p \leq 0.01$ (**), $p \leq 0.001$ (***).

the bone homeostasis, Razzi et al. [20] studied the immunomodulatory potential of PEO-modified AM implants with or without AgNPs by the use of a monoculture. As expected, PEO-treated implants revealed a reduction in the pro-inflammatory response of macrophages and a higher pro-repair response comparing to untreated Ti implants after 4 days of culture, indicating that the topographical and chemical changes resulting from the PEO process, including the presence of micro-/nano-porosity and incorporation of Ca and P elements from the electrolyte promoted the immunomodulatory potential of the surfaces. Nevertheless, a cytotoxic effect of PEO + AgNPs implants towards macrophages was observed. The follow-up study performed by van Poll et al. [37] established that 0.3g/L was the optimal AgNPs concentration with which implants should be fabricated to sufficiently prevent bacterial growth while not impairing macrophage viability. This value is 10 folds smaller than what was used in previous studies. Van Poll et al. discovered that the introduction of AgNPs on implants in a dose dependent manner triggered a similar macrophage polarization pattern as compared to non-silver including implants and additionally did not observe any cytotoxic effects for hMSCs in a short-term. In this study the effects of macrophage polarization induced by AM PEO + 0.3g/L AgNPs biofunctionalized implants on hMSCs osteogenic differentiation and matrix mineralization were evaluated, specifically focusing on assessing the paracrine communication existing between macrophages and hMSCs in the new bone formation process around the biomaterial. Therefore, a co-culture model was developed.

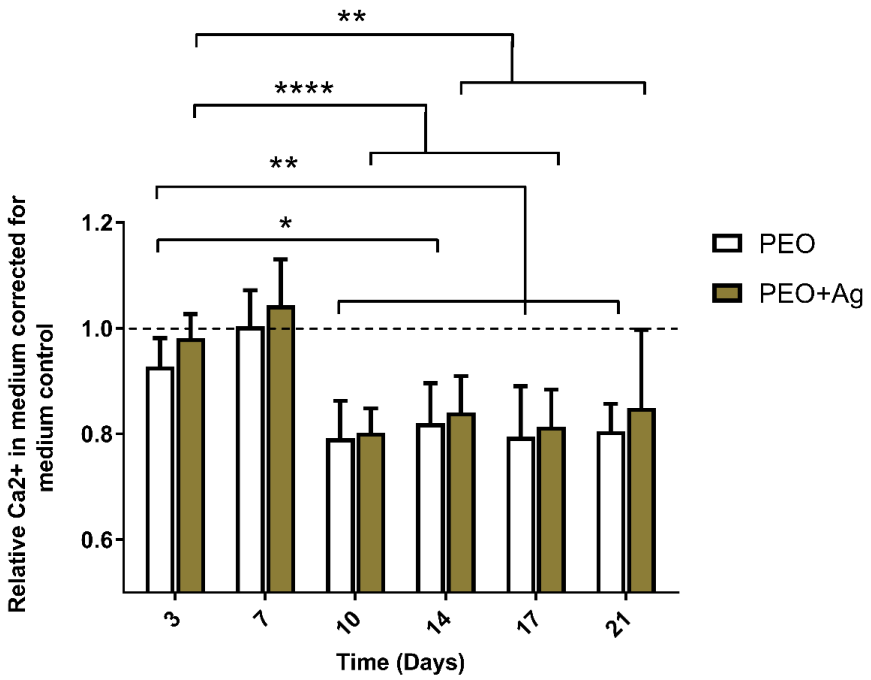

Figure 19. ECM mineralization of hMSCs co-cultured with macrophages. Relative Ca^{2+} concentration in culture medium for hMSCs cultured on implant surfaces over a period of 21 days. $p \leq 0.05$ (*), $p \leq 0.01$ (**), $p \leq 0.0001$ (****).

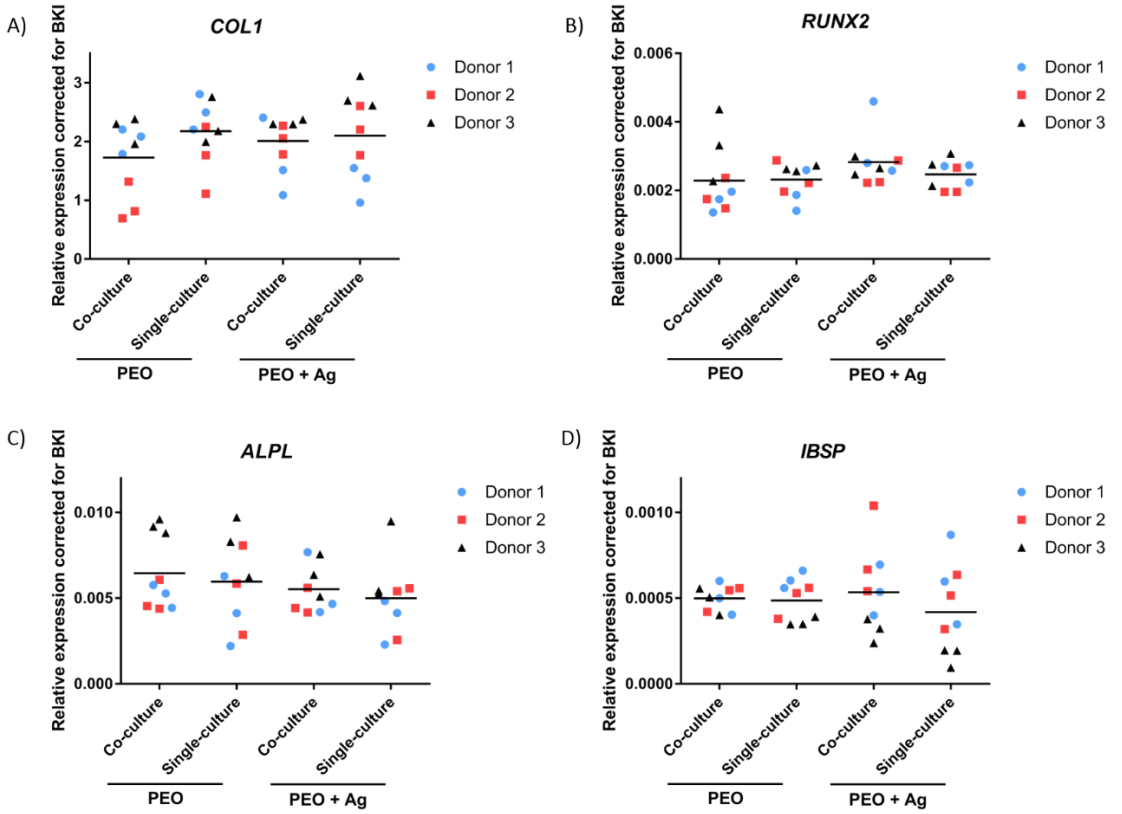

Figure 20. Gene expression levels of osteogenesis-related genes in hMSCs cultured on implant surfaces in single- or co-culture after 7 days in osteogenic induction medium.

4.1 Effects of PEO biofunctionalization on implant surface characteristics

AM titanium implants were biofunctionalized by means of a PEO treatment. Two different electrolytes were employed, with or without AgNPs but both containing calcium acetate and calcium glycerophosphate. This resulted in two types of surfaces (PEO and PEO + Ag) with similar topographical features but different chemical composition. PEO biofunctionalization led to an increase in the surface roughness by the creation of TiO_2 layers with interconnected micro-/nano-porosity. In addition, the Ag ion release profile confirmed the successful incorporation of AgNPs in the PEO + Ag implant surface. Previous studies from our team also showed the presence of electrolyte elements in the PEO-treated biomaterials such as Ca, P detected by energy dispersive x-ray spectroscopy (EDS)[20], which are known to have beneficial effects on bone formation. Other specific phases that are generated in the PEO biofunctionalization process were also previously detected by X-ray diffraction (XRD) such as polymorphs of TiO_2 including anatase and rutile or calcium phosphates including HA and $Ca_3(PO_4)_2$ [34].

4.2 Ability of hMSCs to osteogenically differentiate on PEO/ PEO + Ag implant surfaces

The first step of this work was to study the long-term effects of PEO + Ag modified implants in hMSCs by means of a monoculture, specifically evaluating if these surfaces could support the osteogenic differentiation of hMSCs and matrix mineralization. As mentioned before, this was previously assessed by our team but only on a short-term basis and focusing solely on the cell viability rather than also assessing their osteogenic ability. Results showed a significant gradual increase of the cell ECM mineralization in both PEO and PEO + Ag treated implants, evidenced by an increase in the calcium uptake of the cells over a period of 17 days until stabilizing its values around day 21. From that time onwards the calcium crystals started growing. SEM imaging of cells at day 24 showed that hMSCs were able to proliferate and attach all over the implant surface forming an abundance of matrix. In addition, the formed calcium deposits were observed at day 31, revealing that both types of implants can promote the formation of calcium nodules as observed by their presence all over the implant surfaces. Analysis of gene expression at day 7 revealed that early and late osteogenic genes were equally expressed in both implant groups, suggesting that they could support the hMSCs osteogenic differentiation and confirming the previous macroscopic results. MSC osteogenic differentiation begins by the proliferation and commitment of these stem cells into pre-osteoblasts [49], a process promoted by early osteogenic markers like *RUNX2*. This gene is known to start its expression in pre-osteoblasts, it is upregulated in immature osteoblasts and finally downregulated in mature osteoblasts [50]. Fully differentiated cells then start synthetizing the ECM by the expression of genes such as *COL-1*. Eventually, the ECM mineralizes in later stages by the help of genes like *IBSP* or *ALPL*. These findings are consistent with previous literature indicating that AgNPs do not present cytotoxic effects on hMSCs when directly applied on top of the cells at low concentrations ($\leq$ 0.01 g/L) and do not compromise the osteogenic differentiation of hMSCs [51, 52]. In addition, they confirm the important role of surface micropores formed by PEO biofunctionalization in creating a strong bond between the biomaterial and bone forming cells as previously observed [53].

4.3 Osteoimmunomodulatory abilities of PEO/PEO + Ag surfaces

Successful new bone formation around the implant in the body strongly depends on the type of immune reaction triggered by the biomaterial. Therefore, the next step of this work was to study the effect of macrophages on hMSCs by means of an indirect co-culture model, in which paracrine communications between both types of cells were investigated. Immediately after the surgical implantation of a biomaterial in the body an acute inflammatory response happens where immune cells such as monocytes are recruited and differentiated into macrophages. In the early stages of the bone repair mechanism, the majority of macrophages are closer to the M1-like phenotype, in order to eliminate pathogens, dead cells and debris and enhance inflammation. Although M1 macrophages help in the attraction of tissue repair cells such as MSCs [54, 55] a persistent pro-inflammatory cytokine presence can lead to the development of fibrotic tissue and biomaterial encapsulation [23]. On the contrary, a correct switching time between a majority of M1 to a majority of M2-like anti-inflammatory macrophages results in a release of osteogenesis-enhancing cytokines that eventually lead to the successful new bone formation around the biomaterial. These polarization changes can be modulated by the biomaterial surface properties because macrophages are known to be sensitive to environmental cues [27].

In terms of the macrophage polarization induced by PEO/PEO + Ag implants, results were comparable to those previously observed by van Poll et al [37]. IL6, used in this study as a pro-inflammatory marker, was similarly expressed in PEO and PEO + Ag groups on both gene and protein levels. This factor is mostly secreted by M1-like macrophages and is known to activate the expression of RANKL, a factor very involved in osteoclastogenesis [56, 57]. However, some pieces of contrasting data recently found that IL6 may also have an important role in the callus maturity in the early stages of fracture healing [58]. Guihard et al. observed MSCs osteogenesis via OSM secretion by M1-like macrophages [59]. This pro-osteogenic cytokine belongs to the IL6 family [60] and in this study comparable low expression levels were measured in both PEO and PEO + Ag specimens. Another gene reported to promote the osteogenic differentiation of MSCs is *PTGS2* [28]. Pro-inflammatory M1 macrophages were found to enhance MSC osteogenesis and bone formation early in the process via the PTGS2-Prostaglandin E2 pathway [61]. This gene was also similarly expressed in both biomaterial groups in this study. On the contrary, tissue-repair chemokine CCL18 was observed to be upregulated in PEO implants compared to PEO + Ag in both gene and protein level. The same tendency was observed for surface marker CD163, characteristic of anti-inflammatory M2-like macrophages which downregulate the pro-inflammatory factors [62]. These results indicate that the presence of AgNPs on implant surfaces might slightly compromise the pro-repair behaviour of macrophages or possibly delay the onset of the tissue repair phase. Nevertheless, it is important to note that only two genes expressed by M2-like macrophages were analysed in this work and at one specific timepoint. Further investigation is needed in order to better understand the macrophage polarization induced by PEO/PEO + Ag in short- and long-term.

Possible paracrine effects of polarized macrophages stimulated by PEO/PEO + Ag surfaces on hMSCs were investigated by analysing the expression of genes associated with osteogenesis (*RUNX2*, *COL-1*, *IBSP* and *ALPL*) after 3 days of co-culture and 7 days of single-culture. No differences in the expression of these genes were observed between PEO and PEO + Ag specimens as well as for the same groups in co-culture or single-culture. These findings confirm the positive osteogenic properties of PEO/PEO + Ag surfaces as previously observed when culturing hMSCs on implant surfaces in a monoculture, but suggest that they

might elicit a limited immunomodulation in order to have an effect on the hMSC mineralization. These results are inconsistent with previous findings in literature, which reported enhanced osteogenic properties of osteoblastic cells cultured with macrophages on PEO biofunctionalized [36, 63–67] or AgNPs incorporated [68] titanium surfaces. Considering the complex surface properties of PEO and PEO + Ag surfaces, it is most likely that both surface physical and chemical properties played an equally essential role in modulating the behaviour of macrophages in this study. In terms of topography, despite the limited number of studies recently published on the PEO modified surfaces, increasing the nanoscale roughness of micro/nano rough surfaces via a post heat-treatment was reported to enhance the biofunctionality of implants and increase the macrophage attachment, proliferation and secretion of pro-osteogenic factors, comparing with those PEO surfaces with no heat treatment and thus limited nanotopography [63, 64, 67]. The underlying mechanism of the effect of these surfaces on these cells is yet not fully known, but studies suggested the importance of mechanotransduction. For example, Pan et al. [18] hypothesized that the nanotopography elicited effects on the macrophage morphology via the increase of the cytoskeleton tension, which switched their phenotype to M2 and promoted the release of the osteogenic factor BMP2. This factor was undetectable in this study. In addition, in terms of chemical properties, the heat treatment also increased the hydrophilicity, hybrid rutile/anatase components and improved HA crystallinity, which contributed to the overall osteoimmunomodulatory properties of the implants. Therefore, it might be interesting to consider investigating some of those strategies that can be incorporated into PEO biofunctionalization with the aim of promoting the osteo-immune environment in future research projects.

Another possible explanation for this observed limited osteoimmunomodulatory behaviour could be related to the co-culture experimental design. The cell culture model developed in this study was carefully planned in order to closely mimic the *in vivo* wound healing process. First, monocytes alone were incubated on the implant surfaces for 48 hours and after which they were put into contact with hMSCs in the same dish. Macrophage polarization and hMSCs mineralization were investigated at the timepoints that were thought most representative of the entirety of the process. However, future research should include more time points along a longer time course, in order to have a clearer and broader picture of the effect of PEO + Ag treated implants on macrophages/hMSCs interactions. In addition, the wound healing process is characterised by a bidirectional macrophage/MSCs direct cell-cell and paracrine contact. This study focused on studying the one-way macrophage effect on hMSCs, specifically focusing on the paracrine communications. Nevertheless, both ways must be considered in order to better approximate to the *in vivo* situation. Previous studies have reported the creation of an *in vitro* osteo-immune environment via the positive feedback existing between macrophages and MSCs, speculating that the macrophage expression of the pro-osteogenic gene *PTGS2* improved the mineralization of MSCs and increased their expression of *PTGS2*, which subsequently improved the anti-inflammatory polarization of macrophages [28]. Finally, macrophage/MSCs paracrine as well as direct communications should also be further studied, which would probably involve the modification of the current "indirect" model into a more "direct" model where cells would be able to interact via cytokine/chemokine secretion as well as direct cell-cell communication.

All in all, despite PEO + Ag surfaces did not produce an immunomodulation that enhanced hMSCs osteogenic differentiation in this study, these surfaces also did not detrimentally change the macrophage response and their paracrine effects on hMSCs, making them very good candidates for achieving osteoimmunomodulatory properties.

4.4 Recommendations for future work

In this study limited osteoimmunomodulatory properties of PEO + Ag surfaces were observed by a lack of enhancement of the hMSCs osteogenic differentiation co-cultured with macrophages. However, no inhibition was also reported. Therefore, further research is needed in order to obtain a clearer picture of the actual potential of the surfaces to elicit an immune reaction that has the ability to modulate the mineralization of hMSCs. Some of the aspects that can be investigated in future studies are the following:

- Perform further characterization of PEO treated surfaces in order to expand the knowledge on the mechanisms that may be most important on modulating the macrophage response. Atomic force microscopy can be used to quantify the roughness or the water contact angle for the wettability.

- Investigate the possibility of other surface biofunctionalization techniques that can be combined with PEO in order to increase their biofunctionality, such as heat treatment or incorporation of HA particles.

- Study a wider amount of pro-inflammatory, anti-inflammatory and pro-osteogenic factors secreted by macrophages at more timepoints and a longer period of time. This would enable to understand better the effect of PEO + Ag surfaces on the macrophage behaviour over time.

- Study the hMSCs mineralization by gene expression at more timepoints and a longer time course.

- Further optimize the number of cells present on the co-culture dish in order to maximize the chances of establishing cell communication.

- Explore other co-culture models such as a transwell model or a direct model. The latter would enable to study both the paracrine and direct cell-cell communications.

- Study both directions of the macrophage/hMSCs communications in order to better understand their interactions.

- Investigate the PEO + Ag implants in an *ex vivo* and *in vivo* context.

5. CONCLUSIONS

This study aimed to investigate the osteoimmunomodulatory properties of PEO + Ag surfaces. For that purpose, AM titanium implants were fabricated and biofunctionalized by means of a PEO treatment with or without AgNPs. The generated surfaces showed the presence of interconnected micro and nanoporosities on a layer of TiO_2 and the successful incorporation of Ag was confirmed by an Ag ion release analysis. The culture of hMSCs on these implants revealed their successful role on supporting the osteogenic differentiation and the presence of AgNPs did not compromise the osteogenesis process. The macrophages co-cultured with hMSCs showed no big differences in their polarization pattern when cultured on PEO or PEO + Ag surfaces. In addition, the amount of cytokines and chemokines they secreted did not result in an enhancement of the hMSCs osteogenic differentiation. This might be attributed to the limited nanoporosities present on these surfaces, which were found to increase macrophage adhesion, morphology and pro-osteogenic cytokine secretion. Nevertheless, data reported in this study also showed no detrimental effects of PEO + Ag surfaces on the macrophage response and their paracrine effects on hMSCs, making them promising candidates for achieving dual antibacterial and osteoimmunomodulatory properties. Future strategies to improve PEO-treated implant surface characteristics might help on the creation of an osteogenesis-enhancing osteo-immune environment where bone could be successfully formed by the positive mediation of the macrophage action. In addition, considering the limitations of the co-culture system built in this study, future studies should also focus on optimizing the current co-culture system and/or developing a novel model associated with more detailed investigations including more time points and cellular markers.

LIST OF ABBREVIATIONS

AgNPs	Silver nanoparticles
ALPL	Alkaline phosphatase
AM	Additive manufacturing
B2M	Beta-2-Microglobulin
BKI	Best keeper index
BMP2	Bone Morphogenetic Protein 2
BSA	Bovine serum albumina
Ca	Calcium
CaA	Calcium acetate
$CaCl_2$	Calciumchloride
CaGly	Calcium glycerophophate
CCL18	Chemokine (c-c motif) ligand 18
CD163	Cluster of differentiation 163
cDNA	Complementary DNA
CO_2	Carbon dioxide
COL-I	Collagen type I
ECM	Extracellular matrix
EDS	X-ray spectroscopy
ELISA	Enzyme-linked immunosorbent assay
FBS	Fetal bovine serum
FGF_2	Fibroblast growth factor-2
GAPDH	Glyceraldehyde-3-phosphate dehydrogenase
hMSCs	Human mesenchymal stem cells
HA	Hydroxyapatite
IAI	Implant associated infections
IBSP	Integrin binding sialoprotein
ICP-OES	Inductively coupled plasma - optical emission spectrometry
IL6	Interleukin 6
MACS	Magnetic-activated cell sorting
MAO	Micro-arc oxidation

MSCs	Mesenchymal stem cells
OSM	Oncostatin M
PEO	Plasma electrolytic oxidation
P	Phosphate
PBS	Phophate buffer saline
PBMCs	Peripheral blood mononuclear cells
PFA	Paraformaldehyde
PTGS2	Prostaglandin-endoperoxide synthase 2
qPCR	Quantitative polymerase chain reaction
RUNX2	Runt-related transcription factor 2
RT	Reverse transcription
RT-qPCR	Reverse transcription quantitative polymerase chain reaction
SED	Secondary electron detector
SLM	Selective laser melting
UBC	Ubiquitin C
TiO_2	Titanium oxide

6. BIBLIOGRAPHY

[1] K. Markatos, G. Tsoucalas, and M. Sgantzos, "Hallmarks in the history of orthopaedic implants for trauma and joint replacement.," *Acta medico-historica adriatica : AMHA*, vol. 14, no. 1, pp. 161–76, 2016, [Online]. Available: http://www.ncbi.nlm.nih.gov/pubmed/27598960.

[2] F. Korkusuz, *Musculoskeletal Research and Basic Science*. Springer, 2016.

[3] M. Özcan and C. Hämmerle, "Titanium as a reconstruction and implant material in dentistry: Advantages and pitfalls," *Materials*, vol. 5, no. 9, pp. 1528–1545, 2012, doi: 10.3390/ma5091528.

[4] D. A. Register, "LROI Annual Report 2019," *Dutch Athroplasty Register (LROI)*, 2019.

[5] J. Tedesco *et al.*, "Osseointegration of a 3D Printed Stemmed Titanium Dental Implant: A Pilot Study," *International Journal of Dentistry*, vol. 2017, 2017, doi: 10.1155/2017/5920714.

[6] C. Agrawal, J. Ong, M. Appleford, and G. Mani, *Introduction to Biomaterials: Basic Theory with Engineering Applications*. Cambridge, UK: Cambridge University Press, 2013.

[7] L. Yuan, S. Ding, and C. Wen, "Additive manufacturing technology for porous metal implant applications and triple minimal surface structures: A review," *Bioactive Materials*, vol. 4, no. 1, pp. 56–70, 2019, doi: 10.1016/j.bioactmat.2018.12.003.

[8] N. Taniguchi *et al.*, "Effect of pore size on bone ingrowth into porous titanium implants fabricated by additive manufacturing: An in vivo experiment," *Materials Science and Engineering C*, vol. 59, pp. 690–701, 2016, doi: 10.1016/j.msec.2015.10.069.

[9] A. A. Zadpoor, "Bone tissue regeneration: The role of scaffold geometry," *Biomaterials Science*, vol. 3, no. 2, pp. 231–245, 2015, doi: 10.1039/c4bm00291a.

[10] S. M. Ahmadi *et al.*, "Additively manufactured open-cell porous biomaterials made from six different space-filling unit cells: The mechanical and morphological properties," *Materials*, vol. 8, no. 4, pp. 1871–1896, 2015, doi: 10.3390/ma8041871.

[11] M. F. Pittenger, D. E. Discher, B. M. Péault, D. G. Phinney, J. M. Hare, and A. I. Caplan, "Mesenchymal stem cell perspective: cell biology to clinical progress," *npj Regenerative Medicine*, vol. 4, no. 1, 2019, doi: 10.1038/s41536-019-0083-6.

[12] E. Matykina, P. Skeldon, and G. E. Thompson, "Fundamental and practical evaluation of plasma electrolytic oxidation coatings of titanium," *Surface Engineering*, vol. 23, no. 6, pp. 412–418, 2007, doi: 10.1179/174329407X247154.

[13] I. A. J. van Hengel *et al.*, "Biofunctionalization of selective laser melted porous titanium using silver and zinc nanoparticles to prevent infections by antibiotic-resistant bacteria," *Acta Biomaterialia*, vol. 107, pp. 325–337, 2020, doi: 10.1016/j.actbio.2020.02.044.

[14] C. K. Wei and S. J. Ding, "Dual-functional bone implants with antibacterial ability and osteogenic activity," *Journal of Materials Chemistry B*, vol. 5, no. 10, pp. 1943–1953, 2017, doi: 10.1039/c7tb00173h.

[15] J. Zhou, X. Wang, and L. Zhao, "Antibacterial, angiogenic, and osteogenic activities of Ca, P, Co, F, and Sr compound doped titania coatings with different Sr content," *Scientific Reports*, vol. 9, no. 1, pp. 1–11, 2019, doi: 10.1038/s41598-019-50496-3.

[16] X. Shen *et al.*, "Antibacterial and Osteogenic Functionalization of Titanium With Silicon/Copper-Doped High-Energy Shot Peening-Assisted Micro-Arc Oxidation Technique," *Frontiers in Bioengineering and Biotechnology*, vol. 8, no. October, pp. 1–13, 2020, doi: 10.3389/fbioe.2020.573464.

[17] I. A. J. van Hengel *et al.*, "Functionality-packed additively manufactured porous titanium implants," *Materials Today Bio*, vol. 7, no. May, pp. 1–12, 2020, doi: 10.1016/j.mtbio.2020.100060.

[18] H. Pan *et al.*, "Immunomodulation effect of a hierarchical macropore/nanosurface on osteogenesis and angiogenesis," *Biomedical Materials (Bristol)*, vol. 12, no. 4, 2017, doi: 10.1088/1748-605X/aa6b7c.

[19] Y. Xie *et al.*, "Osteoimmunomodulatory effects of biomaterial modification strategies on macrophage polarization and bone regeneration," *Regenerative Biomaterials*, vol. 7, no. 3, pp. 233–245, 2020, doi: 10.1093/rb/rbaa006.

[20] F. Razzi *et al.*, "Immunomodulation of surface biofunctionalized 3D printed porous titanium implants," *Biomedical Materials (Bristol)*, vol. 15, no. 3, May 2020, doi: 10.1088/1748-605X/ab7763.

[21] J. M. Anderson, A. Rodriguez, and D. T. Chang, "Foreign body reaction to biomaterials," *Seminars in Immunology*, vol. 20, no. 2, pp. 86–100, 2008, doi: 10.1016/j.smim.2007.11.004.

[22] M. Scarritt, R. Londono, and S. F. Badylak, "Host Response to Implanted Materials and Devices: An Overview," in *The Immune Response to Implanted Materials and Devices*, B. Corradetti, Ed. Springer, 2017, pp. 1–14.

[23] L. Davenport Huyer, S. Pascual-Gil, Y. Wang, S. Mandla, B. Yee, and M. Radisic, "Advanced Strategies for Modulation of the Material–Macrophage Interface," *Advanced Functional Materials*, vol. 30, no. 44, pp. 1–21, 2020, doi: 10.1002/adfm.201909331.

[24] B. V. Fearing and M. E. Van Dyke, "In vitro response of macrophage polarization to a keratin biomaterial," *Acta Biomaterialia*, vol. 10, no. 7, pp. 3136–3144, 2014, doi: 10.1016/j.actbio.2014.04.003.

[25] D. M. Mosser and J. P. Edwards, "Exploring the full spectrum of macrophage activation," *Nature Reviews Immunology*, vol. 8, no. 12, pp. 958–969, 2008, doi: 10.1038/nri2448.

[26] Z. Chen *et al.*, "Osteoimmunomodulation for the development of advanced bone biomaterials," *Materials Today*, vol. 19, no. 6, pp. 304–321, 2016, doi: 10.1016/j.mattod.2015.11.004.

[27] A. Sica, P. Invernizzi, and A. Mantovani, "Macrophage plasticity and polarization

in liver homeostasis and pathology," *Hepatology*, vol. 59, no. 5, pp. 2034–2042, 2014, doi: 10.1002/hep.26754.

[28] L. Chen *et al.*, "Synergistic effects of immunoregulation and osteoinduction of ds-block elements on titanium surface," *Bioactive Materials*, vol. 6, no. 1, pp. 191–207, 2021, doi: 10.1016/j.bioactmat.2020.08.001.

[29] J. Lee, H. Byun, S. K. Madhurakkat Perikamana, S. Lee, and H. Shin, "Current Advances in Immunomodulatory Biomaterials for Bone Regeneration," *Advanced Healthcare Materials*, vol. 8, no. 4. Wiley-VCH Verlag, Feb. 21, 2019, doi: 10.1002/adhm.201801106.

[30] K. M. Hotchkiss, G. B. Reddy, S. L. Hyzy, Z. Schwartz, B. D. Boyan, and R. Olivares-Navarrete, "Titanium surface characteristics, including topography and wettability, alter macrophage activation," *Acta Biomaterialia*, vol. 31, pp. 425–434, 2016, doi: 10.1016/j.actbio.2015.12.003.

[31] S. M. Hamlet, R. S. B. Lee, H. J. Moon, M. A. Alfarsi, and S. Ivanovski, "Hydrophilic titanium surface-induced macrophage modulation promotes pro-osteogenic signalling," *Clinical Oral Implants Research*, vol. 30, no. 11, pp. 1085–1096, 2019, doi: 10.1111/clr.13522.

[32] T. Kado, H. Aita, Y. Ichioka, K. Endo, and Y. Furuichi, "Chemical modification of pure titanium surfaces to enhance the cytocompatibility and differentiation of human mesenchymal stem cells," *Dental Materials Journal*, vol. 38, no. 6, pp. 1026–1035, 2019, doi: 10.4012/dmj.2018-257.

[33] D. Ingrassia, M. Sladkova, M. Palmer, W. Xia, H. Engqvist, and G. M. de Peppo, "Stem cell-mediated functionalization of titanium implants," *Journal of Materials Science: Materials in Medicine*, vol. 28, no. 9, 2017, doi: 10.1007/s10856-017-5944-1.

[34] I. A. J. van Hengel *et al.*, "Selective laser melting porous metallic implants with immobilized silver nanoparticles kill and prevent biofilm formation by methicillin-resistant Staphylococcus aureus," *Biomaterials*, vol. 140, pp. 1–15, 2017, doi: 10.1016/j.biomaterials.2017.02.030.

[35] J. Bai *et al.*, "Biomimetic osteogenic peptide with mussel adhesion and osteoimmunomodulatory functions to ameliorate interfacial osseointegration under chronic inflammation," *Biomaterials*, vol. 255, no. June, p. 120197, 2020, doi: 10.1016/j.biomaterials.2020.120197.

[36] Q. Huang, Z. Ouyang, Y. Tan, H. Wu, and Y. Liu, "Activating macrophages for enhanced osteogenic and bactericidal performance by Cu ion release from micro/nano-topographical coating on a titanium substrate," *Acta Biomaterialia*, vol. 100, pp. 415–426, 2019, doi: 10.1016/j.actbio.2019.09.030.

[37] M. Van Poll, L. Fratila-Apachitei, E. Farrell, N. Fahy, and A. A. Zadpoor, "Effects of silver nanoparticle-containing 3D printed antibacterial implants on macrophages." 2019, [Online]. Available: https://repository.tudelft.nl/islandora/object/uuid%3A0abd5c96-4675-423a-a12a-9c0ab16d1246.

[38] B. L. Jiang and Y. M. Wang, "Plasma electrolytic oxidation treatment of aluminium and titanium alloys," *Surface Engineering of Light Alloys: Aluminium,*

Magnesium and Titanium Alloys, pp. 110–154, 2010, doi: 10.1533/9781845699451.2.110.

[39] L. Zhu *et al.*, "Microstructure and corrosion resistance of the PEO coating on extruded Al6Cu alloy," *Surface and Coatings Technology*, vol. 369, no. August 2018, pp. 116–126, 2019, doi: 10.1016/j.surfcoat.2019.04.027.

[40] I. A. J. Van Hengel *et al.*, "Self-defending additively manufactured bone implants bearing silver and copper nanoparticles," *Journal of Materials Chemistry B*, vol. 8, no. 8, pp. 1589–1602, 2020, doi: 10.1039/c9tb02434d.

[41] A. Fattah-alhosseini, K. Babaei, and M. Molaei, "Plasma electrolytic oxidation (PEO) treatment of zinc and its alloys: A review," *Surfaces and Interfaces*, vol. 18, no. January, p. 100441, 2020, doi: 10.1016/j.surfin.2020.100441.

[42] C. A. Knuth *et al.*, "Isolating Pediatric Mesenchymal Stem Cells with Enhanced Expansion and Differentiation Capabilities," *Tissue Engineering - Part C: Methods*, vol. 24, no. 6, pp. 313–321, 2018, doi: 10.1089/ten.tec.2018.0031.

[43] I. J. Fuss, M. E. Kanof, P. D. Smith, and H. Zola, "Isolation of whole mononuclear Cells from peripheral blood and cord blood," *Current Protocols in Immunology*, no. SUPPL. 85, pp. 1–8, 2009, doi: 10.1002/0471142735.im0701s85.

[44] STEMCELL technologies, "Isolate Cells from Blood | Cell Separation Techniques." https://www.stemcell.com/cell-separation/isolate-cells-from-blood.

[45] B. A. Rahn and S. M. Perren, "Xylenol orange, a fluorochrome useful in polychrome sequential labeling of calcifying tissues," *Stain technology*, vol. 4, no. 3, pp. 125–129, 1971.

[46] Thermo Fisher Scientific, "Reverse Transcription Applications." https://www.thermofisher.com/nl/en/home/life-science/cloning/cloning-learning-center/invitrogen-school-of-molecular-biology/rt-education/reverse-transcription-applications.html.

[47] "Sandwich ELISA Protocol - Leinco Technologies." https://www.leinco.com/sandwich-elisa-protocol/.

[48] Invitrogen, "CyQUANT Cell Proliferation Assay Kit | Molecular Probes; invitrogen detection technologies," p. 7, 2006.

[49] R. D. A. M. Alves, *Osteoblast differentiation and bone: Relevant proteins, regulatory processes and the vascular connection (PhD Thesis)*. Rotterdam: Erasmus University Rotterdam, 2012.

[50] Z. Tang, X. Li, Y. Tan, H. Fan, and X. Zhang, "The material and biological characteristics of osteoinductive calcium phosphate ceramics," *Regenerative Biomaterials*, vol. 5, no. 1, pp. 43–59, 2018, doi: 10.1093/rb/rbx024.

[51] L. Pauksch *et al.*, "Biocompatibility of silver nanoparticles and silver ions in primary human mesenchymal stem cells and osteoblasts," *Acta Biomaterialia*, vol. 10, no. 1, pp. 439–449, 2014, doi: 10.1016/j.actbio.2013.09.037.

[52] C. Sengstock, J. Diendorf, M. Epple, T. A. Schildhauer, and M. Köller, "Effect of silver nanoparticles on human mesenchymal stem cell differentiation," *Beilstein Journal of Nanotechnology*, vol. 5, no. 1, pp. 2058–2069, 2014, doi:

10.3762/bjnano.5.214.

[53] P. Xiu *et al.*, "Tailored Surface Treatment of 3D Printed Porous Ti6Al4V by Microarc Oxidation for Enhanced Osseointegration via Optimized Bone In-Growth Patterns and Interlocked Bone/Implant Interface," *ACS Applied Materials and Interfaces*, vol. 8, no. 28, pp. 17964–17975, 2016, doi: 10.1021/acsami.6b05893.

[54] J. long Sun *et al.*, "Intrafibrillar silicified collagen scaffold modulates monocyte to promote cell homing, angiogenesis and bone regeneration," *Biomaterials*, vol. 113, pp. 203–216, 2017, doi: 10.1016/j.biomaterials.2016.10.050.

[55] C. Shi and E. G. Pamer, "Monocyte recruitment during infection and inflammation," *Nature Reviews Immunology*, vol. 11, no. 11, pp. 762–774, 2011, doi: 10.1038/nri3070.

[56] F. Yoshitake, S. Itoh, H. Narita, K. Ishihara, and S. Ebisu, "Interleukin-6 directly inhibits osteoclast differentiation by suppressing receptor activator of NF-κB signaling pathways," *Journal of Biological Chemistry*, vol. 283, no. 17, pp. 11535–11540, 2008, doi: 10.1074/jbc.M607999200.

[57] M. H. Abdel Meguid, Y. H. Hamad, R. S. Swilam, and M. S. Barakat, "Relation of interleukin-6 in rheumatoid arthritis patients to systemic bone loss and structural bone damage," *Rheumatology International*, vol. 33, no. 3, pp. 697–703, 2013, doi: 10.1007/s00296-012-2375-7.

[58] X. Yang, B. F. Ricciardi, A. Hernandez-Soria, Y. Shi, N. Pleshko Camacho, and M. P. G. Bostrom, "Callus mineralization and maturation are delayed during fracture healing in interleukin-6 knockout mice," *Bone*, vol. 41, no. 6, pp. 928–936, 2007, doi: 10.1016/j.bone.2007.07.022.

[59] P. Guihard *et al.*, "Induction of osteogenesis in mesenchymal stem cells by activated monocytes/macrophages depends on oncostatin M signaling," *Stem Cells*, vol. 30, no. 4, pp. 762–772, 2012, doi: 10.1002/stem.1040.

[60] A. Grenier *et al.*, "Oncostatin M production and regulation by human polymorphonuclear neutrophils," *Blood*, vol. 93, no. 4, pp. 1413–1421, 1999, doi: 10.1182/blood.v93.4.1413.

[61] L. Y. Lu *et al.*, "Pro-inflammatory M1 macrophages promote Osteogenesis by mesenchymal stem cells via the COX-2-prostaglandin E2 pathway," *Journal of Orthopaedic Research*, vol. 35, no. 11, pp. 2378–2385, 2017, doi: 10.1002/jor.23553.

[62] P. A. Rees, N. S. Greaves, M. Baguneid, and A. Bayat, "Chemokines in Wound Healing and a[1] P. A. Rees, N. S. Greaves, M. Baguneid, and A. Bayat, 'Chemokines in Wound Healing and as Potential Therapeutic Targets for Reducing Cutaneous Scarring,' Advances in Wound Care, vol. 4, no. 11, pp. 687–703, 2015, doi: ," *Advances in Wound Care*, vol. 4, no. 11, pp. 687–703, 2015, doi: 10.1089/wound.2014.0568.

[63] L. Bai *et al.*, "A multifaceted coating on titanium dictates osteoimmunomodulation and osteo/angio-genesis towards ameliorative osseointegration," *Biomaterials*, vol. 162, pp. 154–169, 2018, doi: 10.1016/j.biomaterials.2018.02.010.

[64] L. Bai *et al.*, “Differential effect of hydroxyapatite nano-particle versus nano-rod decorated titanium micro-surface on osseointegration,” *Acta Biomaterialia*, vol. 76, pp. 344–358, 2018, doi: 10.1016/j.actbio.2018.06.023.

[65] Q. Huang *et al.*, “The osteogenic, inflammatory and osteo-immunomodulatory performances of biomedical Ti-Ta metal–metal composite with Ca- and Si-containing bioceramic coatings,” *Colloids and Surfaces B: Biointerfaces*, vol. 169, pp. 49–59, 2018, doi: 10.1016/j.colsurfb.2018.05.010.

[66] X. Li *et al.*, “Evaluating the osteoimmunomodulatory properties of micro-arc oxidized titanium surface at two different biological stages using an optimized in vitro cell culture strategy,” *Materials Science and Engineering C*, vol. 110, no. December 2018, p. 110722, 2020, doi: 10.1016/j.msec.2020.110722.

[67] R. Zhang *et al.*, “The immunomodulatory effects of Zn-incorporated micro/nanostructured coating in inducing osteogenesis,” *Artificial Cells, Nanomedicine and Biotechnology*, vol. 46, no. sup1, pp. 1123–1130, 2018, doi: 10.1080/21691401.2018.1446442.

[68] Y. Chen *et al.*, “Improved immunoregulation of ultra-low-dose silver nanoparticle-loaded TiO2 nanotubes via M2 macrophage polarization by regulating GLUT1 and autophagy,” *International Journal of Nanomedicine*, vol. 15, pp. 2011–2026, 2020, doi: 10.2147/IJN.S242919.

7. APPENDIX

7.1 Implant characteristics: Voltage transients for PEO process monitoring

The PEO process was monitored by means of voltage-time transients (Figure). Results show that voltages increased linearly and rapidly in the initial stages of the modification, due to the thickening of the TiO_2 layer. After 10 seconds the voltage increase slows down, coinciding with the beginning of the dielectric breakdown and formation of the porous layer on the surface of the implants. No difference was found in the V-t graphs between PEO and PEO+Ag samples.

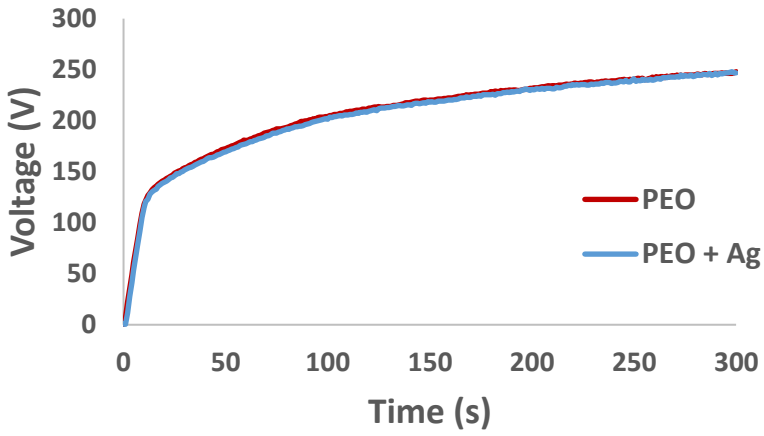

Figure S1. Voltage-time transients recorded during the implant biofunctionalization process.

7.2 Osteogenic differentiation of hMSCs attached to implant surfaces: Calcium concentration in culture medium

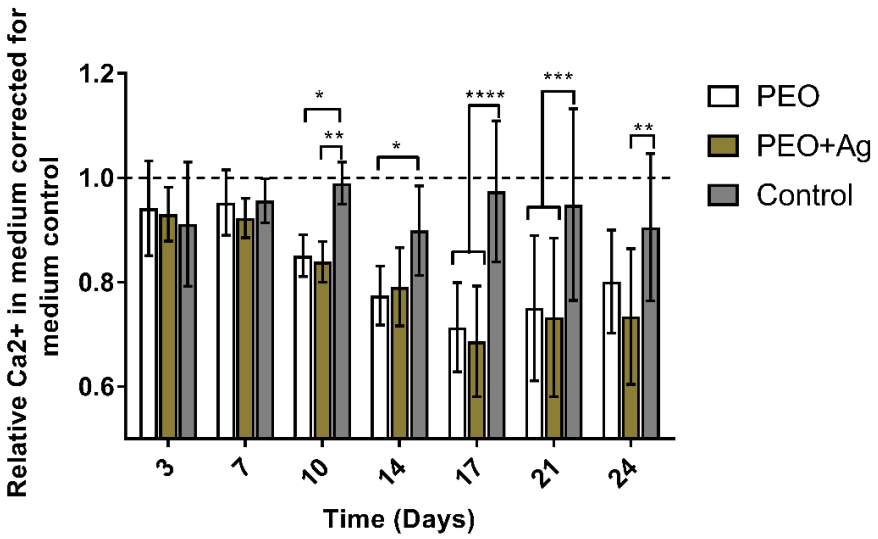

Figure S2. Relative Ca^{2+} concentration in culture medium for hMSCs cultured on PEO, PEO + Ag and control implants over a period of 24 days. $p \leq 0.05$ (*), $p \leq 0.01$ (**), $p \leq 0.001$ (***), $p \leq 0.0001$ (****).

7.3 Cq values of RT-qPCR for gene expression analysis

Table S1. Cq values of genes analysed for the osteogenic evaluation of hMSCs cultured on implant surfaces in a single-culture.

	Gene / Donor	*COL-1*	*RUNX2*	*ALPL*	*IBSP*	*GAPDH*	*B2M*	*UBC*	*BKI index*
PEO	1	16.73	26.51	25.74	29.65	18.93	16.19	18.99	18.04
	2	15.90	25.90	26.80	27.76	18.33	15.61	18.06	17.34
	3	16.26	26.06	25.42	28.02	19.03	16.12	17.35	17.50
PEO + Ag	1	17.01	26.67	26.68	29.73	19.22	15.63	18.26	17.70
	2	16.10	25.82	26.48	27.34	18.71	14.83	18.19	17.24
	3	16.97	26.98	25.89	28.00	19.83	16.84	18.33	18.33

Table S2. Cq values of genes analysed for the immunological evaluation of macrophages cultured on implant surfaces in a co-culture with hMSCs.

	Gene / Donor	*IL6*	*CCL18*	*CD163*	*OSM*	*PTGS2*	*GAPDH*	*B2M*	*UBC*	*BKI index*
PEO	1	28.62	27.47	22.29	27.20	32.69	23.91	18.70	21.91	21.50
	2	35.14	30.97	26.43	34.35	36.71	28.17	23.61	26.93	26.24
	3	33.88	28.15	23.57	29.16	34.91	24.97	20.76	23.18	22.97
PEO + Ag	1	32.11	31.53	25.61	30.09	35.30	26.22	21.34	24.71	24.09
	2	32.30	29.55	24.67	30.59	36.42	25.77	21.20	24.34	23.77
	3	33.66	26.55	22.06	28.08	34.28	22.94	18.78	20.81	20.84

Table S3. Cq values of genes analysed for the osteogenic evaluation of hMSCs cultured on implant surfaces in a co-culture with macrophages.

		Gene / Donor	*COL-1*	*RUNX2*	*ALPL*	*IBSP*	*GAPDH*	*B2M*	*UBC*	*BKI index*
PEO	**Co-culture**	1	16.86	27.10	25.48	28.86	20.35	16.05	17.49	17.96
		2	17.85	26.80	25.37	28.66	19.87	16.27	17.18	17.77
		3	16.21	25.64	24.12	28.37	19.26	15.90	16.90	17.35
	Single-culture	1	16.54	26.90	25.88	28.54	19.96	16.11	17.69	17.92
		2	16.38	25.85	24.70	28.12	18.95	15.67	16.83	17.15
		3	16.24	26.00	24.41	28.87	19.41	15.85	17.05	17.44
PEO + Ag	**Co-culture**	1	16.81	25.75	25.03	28.35	20.09	15.80	16.79	17.56
		2	16.50	26.20	25.26	27.96	19.71	15.91	17.15	17.59
		3	16.00	25.75	24.53	28.88	19.23	15.65	16.76	17.22
	Single-culture	1	17.19	26.15	25.66	28.33	20.02	15.75	17.10	17.62
		2	16.39	26.35	25.37	28.55	19.61	15.98	17.11	17.57
		3	16.20	26.26	24.96	30.36	19.62	16.05	17.39	17.69